



저작자표시-비영리-변경금지 2.0 대한민국

이용자는 아래의 조건을 따르는 경우에 한하여 자유롭게

- 이 저작물을 복제, 배포, 전송, 전시, 공연 및 방송할 수 있습니다.

다음과 같은 조건을 따라야 합니다:



저작자표시. 귀하는 원저작자를 표시하여야 합니다.



비영리. 귀하는 이 저작물을 영리 목적으로 이용할 수 없습니다.



변경금지. 귀하는 이 저작물을 개작, 변형 또는 가공할 수 없습니다.

- 귀하는, 이 저작물의 재이용이나 배포의 경우, 이 저작물에 적용된 이용허락조건을 명확하게 나타내어야 합니다.
- 저작권자로부터 별도의 허가를 받으면 이러한 조건들은 적용되지 않습니다.

저작권법에 따른 이용자의 권리는 위의 내용에 의하여 영향을 받지 않습니다.

이것은 [이용허락규약\(Legal Code\)](#)을 이해하기 쉽게 요약한 것입니다.

[Disclaimer](#)

Master's Thesis

Study on Optical and Electrical Property Changes  
of Molybdenum Diselenide by Reversible  
Hydrogenation

Kyung Yeol Ma

Department of Energy Engineering

Graduate School of UNIST

2016

Study on Optical and Electrical Property Changes  
of Molybdenum Diselenide by Reversible  
Hydrogenation

Kyung Yeol Ma

Department of Energy Engineering

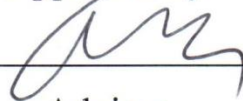
Graduate School of UNIST

# Study on Optical and Electrical Property Changes of Molybdenum Diselenide by Reversible Hydrogenation

A thesis submitted to the Graduate School of UNIST in partial fulfillment  
of the requirements for the degree of Master of Science

1. 13. 2016 Month/Day/Year of submission

Approved by



Advisor

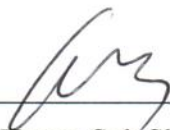
Hyeon Suk Shin

# Study on Optical and Electrical Property Changes of Molybdenum Diselenide by Reversible Hydrogenation

Kyung Yeol Ma


This certifies that the thesis of Kyung Yeol Ma is approved.

1. 13. 2016 Month/Day/Year of submission




---

Advisor: Hyeon Suk Shin



---

Hyunhyub Ko



---

Hyesung Park



## CONTENTS

|   |           |
|---|-----------|
| <i>Contents</i>   | <i>I</i>  |
| <i>List of Figure</i>   | <i>II</i> |
| <i>Abstract</i>   | <i>V</i>  |
| 1. Research Background of Transition Metal Dichalcogenides .....                            | 1         |
| 1.1 Characteristic of Two-Dimensional Transition Metal Dichalcogenides .....                | 3         |
| 1.1.1 Crystal Structure .....   | 3         |
| 1.1.2 Electronic Structure .....  | 4         |
| 1.1.3 Optical Property .....  | 4         |
| 1.2 Isolation or Synthesis Method of Two-Dimensional Transition Metal Dichalcogenides ..... | 9         |
| 1.2.1 Mechanical Exfoliation .....  | 9         |
| 1.2.2 Chemical Exfoliation .....  | 9         |
| 1.2.3 Chemical Vapor Deposition .....   | 10        |
| 1.3 Functionalization of Two-Dimensional Transition Metal Dichalcogenides .....             | 14        |
| 1.3.1 Covalent Functionalization .....  | 14        |
| 1.3.2 Functionalization with Nanoparticles .....  | 15        |
| 1.3.3 Hydrogenation .....   | 15        |
| 2. Experimental Section .....   | 18        |
| 2.1 Synthesis of Single-layer MoSe <sub>2</sub> .....                                       | 18        |
| 2.2 Characterization of Single-layer MoSe <sub>2</sub> .....                                | 18        |
| 2.3 Hydrogenation of MoSe <sub>2</sub> .....  | 18        |
| 2.4 Fabrication of MoSe <sub>2</sub> Field Effect Transistor .....                          | 19        |
| 3. Result and Discussion .....  | 19        |
| 3.1 Surface Characterization of Hydrogenated MoSe <sub>2</sub> .....                        | 19        |
| 3.2 Photoluminescence and Raman of Hydrogenated MoSe <sub>2</sub> .....                     | 24        |
| 3.3 Analysis of X-ray Photoelectron Spectrum on Hydrogenated MoSe <sub>2</sub> .....        | 27        |
| 3.4 Electron Transport Property of Hydrogenated MoSe <sub>2</sub> .....                     | 29        |
| 3.5 Reversible Hydrogenation .....  | 32        |
| 3.6 Hydrogenation of Free-standing MoSe <sub>2</sub> .....                                  | 32        |
| 4. Summary .....  | 35        |
| 5. Reference .....  | 36        |

## List of Figures

**Figure 1.1** The transition metals and the three chalcogen elements that predominantly crystallize in those layered structure are highlighted in the periodic table. Partial highlights for Co, Rh, Ir and Ni indicate that only some of the dichalcogenides from layered structures. For instances, NiS<sub>2</sub> is found to have apyrite structure but NiTe<sub>2</sub> is a layered compound.

**Figure 1.2** (a) side view of bulk MoS<sub>2</sub> (van der Waals bonded MoS<sub>2</sub> units), (b) top view of both bulk MoS<sub>2</sub> and single-layer MoS<sub>2</sub>, (c) side view of single-layer MoS<sub>2</sub>.

**Figure 1.3** Calculated electronic energy band-diagrams are shown for (a) bulk-MoS<sub>2</sub>, (b) 4-layer MoS<sub>2</sub>, (c) 2-layer MoS<sub>2</sub> and (d) single-layer MoS<sub>2</sub>. The solid arrow lines shown in Figure (a), (b) and (c) indicate the indirect transitions from valence band (at  $\Gamma$  point) to the conduction band minimum (along  $\Gamma$ -K direction), whereas in d it indicates the direct electronic transition at the K-point.

**Figure 1.4** (a) Photoluminescence spectra normalized by Raman intensity for MoS<sub>2</sub> layers with different thickness. (b) Raman spectra of single-layer to bulk MoS<sub>2</sub>. The pump radiation was supplied by an Ar ion laser operating at a wavelength of 514.5 nm. The solid line for the 2-layer spectrum is a double Voigt fir by data (circles for 2-layer, solid lines for the rest). (d) Frequencies of E<sub>2g</sub> and A<sub>1g</sub> Raman modes (left vertical axis) and their difference (right vertical axis) as a function of layer number.

**Figure 1.5** Structure and microscopic image of single-layer MoS<sub>2</sub>. (a) Three-dimensional representation of the MoS<sub>2</sub>. (b) Optical image of single-layer MoS<sub>2</sub> deposited on SiO<sub>2</sub> substrate using scotch tape-based mechanical cleavage method. (c) AFM image of a single-layer MoS<sub>2</sub> on SiO<sub>2</sub> substrate. (d) Height profile along the red line in (c).

**Figure 1.6** (a) photographs of dispersed TMD nanosheets and (b) the AFM images corresponded with (a) on SiO<sub>2</sub>. Insets exhibit thickness of nanosheets by height profiles.

**Figure 1.7** Various chemical vapor deposition methods of TMDs. (a) Schematic description of two-step thermolysis, and the obtained MoS<sub>2</sub> films on sapphire and silica substrate. (b) Schematic CVD system of synthesizing single to few-layer MoS<sub>2</sub> by sulfurization of Mo metal thin film. (c) Growth system of single-layer MoS<sub>2</sub> using MoO<sub>3</sub> and S powders by a gas-phase reaction. (d) Wafer-scale synthesis of a few-layer MoS<sub>2</sub> films through direct sulfurization of MoO<sub>3</sub> films. It transfers onto arbitrary substrate.



**Figure 1.8** (a) Scheme of the functionalization strategy (b) Photoluminescence spectra from single-layer 2H-MoS<sub>2</sub> synthesized by CVD, from the metallic 1T-MoS<sub>2</sub> and from the functionalized 1T-MoS<sub>2</sub>. Inset is a CVD-grown single-layer MoS<sub>2</sub> on which the photoluminescence spectra were measured. (c) Modulated photoluminescence with increasing degree of functionalization.

**Figure 1.9** (a) Difference of energy between 1T and 2H-MoS<sub>2</sub> as a function of the attached hydrogen coverage (on S atoms) and calculated band gap of 1T-MoS<sub>2</sub> by different hydrogen coverage. (b) Calculated band gap of 2H-MoS<sub>2</sub> as a function of the number of attached hydrogen atoms. And band structure of pristine 2H-MoS<sub>2</sub> and hydrogenated MoS<sub>2</sub>.

**Figure 2.1** (a) Schematic of the growth setup for synthesizing MoSe<sub>2</sub>. Initial microscopic characterization of single-layer MoSe<sub>2</sub> flakes. (b) Optical image and (c) SEM image of single-layer MoSe<sub>2</sub>. (d) AFM height topography of single-layer MoSe<sub>2</sub> on sapphire. (Inset) Height profile of write line marked in (d).

**Figure 2.2** Initial spectroscopic characterization of single-layer MoSe<sub>2</sub> flakes on sapphire. (a) Raman spectrum and vibration direction of A<sub>1g</sub> and E<sub>2g</sub> mode. (b) PL spectrum. (Inset) PL mapping. (c) UV-vis-NIR spectrum of CVD grown MoSe<sub>2</sub>.

**Figure 2.3** AFM height topography of single-layer MoSe<sub>2</sub> on sapphire (a) before and (b) after 10 minutes hydrogenation. Inset : homogeneous PL peak of single-layer MoSe<sub>2</sub> (a) before and (b) after hydrogenation. (c) Height profile of (a) and (b). MoSe<sub>2</sub> flakes remained intact after H<sub>2</sub> plasma treatment.

**Figure 2.4** PL characterization of hydrogenated MoSe<sub>2</sub>. (a) PL mapping images and (b) PL spectra at center, middle and edge sites of MoSe<sub>2</sub> flakes with different times. (c) PL intensity-time curves at different position. Inset spectra show magnified curves of (c) from 84 seconds to 168 seconds. (d) UV-vis-NIR spectra of before and after hydrogenated MoSe<sub>2</sub> (black line : before, red line : after). (e) Schematic of hydrogenated MoSe<sub>2</sub> at 84 seconds.

**Figure 2.5** (a) Raman spectra of hydrogenated MoSe<sub>2</sub> with different reaction time. (b) Raman spectra of before and after hydrogenated MoSe<sub>2</sub> for 168 seconds.

**Figure 2.6** X-ray photoelectron spectra of single-layer MoSe<sub>2</sub> on platinum substrate before and after hydrogenation (a) XPS spectra of Mo 3d and (b) XPS spectra of Se 3d. Table is comparison of the binding energy of Mo 3d and Se 3d with hydrogenated Mo 3d and Se 3d.

**Figure 2.7** Schematic description of the wet transfer method of MoSe<sub>2</sub> from sapphire to SiO<sub>2</sub>.

**Figure 2.8** (a) AFM height topography of single-layer MoSe<sub>2</sub> on sapphire and (b) on SiO<sub>2</sub> after transfer. (c) Height profiles of (a) and (b).

**Figure 2.9** Schematic description of fabricating the back-gate FET device by E-beam lithography.

**Figure 2.10** Electron transport characteristics from MoSe<sub>2</sub>-based FET device. (a) I-V curves at different gate voltages and (b) I-V<sub>G</sub> curve in MoSe<sub>2</sub>. (c) I-V curves at different gate voltages and (d) I-V<sub>G</sub> curve in hydrogenated MoSe<sub>2</sub> for more than 168 seconds

**Figure 2.11** PL and Raman characteristics of dehydrogenation process. Restored PL and Raman spectra are exhibited in (e), (f) from hydrogenated MoSe<sub>2</sub> (c), (d), respectively. The same positions of PL were emitted between pristine MoSe<sub>2</sub> (a) and dehydrogenated MoSe<sub>2</sub> (e). Also peak of A<sub>1g</sub> mode moves to original position of pristine MoSe<sub>2</sub> (f).

**Figure 2.12** (a) Schematic of one-side and both-side H-MoSe<sub>2</sub>. (b) Raman and (c) PL spectra of both-side H-MoSe<sub>2</sub> with different hydrogenation time. Inset spectra in (b) show magnified E<sub>2g</sub> Raman peak. (d) Normalized PL intensity-time curves of one-side and both-side H-MoSe<sub>2</sub>. Inset in (d) exhibit the magnified curves of from 84 s to 168 s.

## Abstract

Hydrogenation is one of the chemical functionalization methods, which has been investigated as an approach for modulate electronic structure in nanomaterials, since it was theoretically suggested that electronic structure can be modified by degree of hydrogenation of graphene like two-dimensional (2D) materials such as transition metal dichalcogenides (TMDs). In the case of graphene, its electronic structure with zero band-gap has been expected to be opened by surface hydrogenation. Compared to wide researches for hydrogenation reactions on graphene surface, the other 2D materials, ones on TMD was not sufficiently studied. In this thesis, I have studied the surface hydrogenation reaction on TMDs.

Similar to the concept of graphene functionalization, chemical functionalization is known for leading to modification of their electronic and optical properties. Theoretical calculations predicted that the electronic structure of single-layer TMDs also can be tuned by hydrogenation. However, its experimental demonstration has not been realized so far. In addition, TMDs can be used as outstanding catalyst for hydrogen evolution reaction (HER). Therefore, the systematic investigation of hydrogenation on TMDs cannot only unveil the modified electronic structures in TMDs, but also can provide the critical information to understand the interaction between hydrogen atom (or molecule) and TMDs, which is fundamentally important for improving HER efficiency. Here we show modification of electronic properties in MoSe<sub>2</sub>, one of TMD materials, which is synthesized by chemical vapor deposition (CVD) process. The photoluminescence (PL) intensity and peak position indicates a direct band gap of 1.54 eV for the single-layer MoSe<sub>2</sub>. After the hydrogenation by H<sub>2</sub> plasma treatment, semiconducting properties of single-layer MoSe<sub>2</sub> turn into insulator. In a step-by-step PL results, hydrogenation reaction started from edge to center. Also, we confirmed the hydrogen atoms only react with selenium atoms (Se) in X-ray photoelectron spectroscopy (XPS) analysis. This study demonstrates the great potential of controlling electronic property of single-layer MoSe<sub>2</sub> and fundamentally understanding about hydrogenation as a surface functionalization study.

## 1. Research Background of Transition Metal Dichalcogenides

Graphene is the first two-dimensional (2D) atomic crystal, and it is the thinnest substance ever obtained and the strongest material in the world. And it has received a large amount of attention due to its excellent properties and potential for applications in many fields.<sup>1-4</sup> However, the zero bandgap property of graphene has limited its widespread use in viable electronic device applications as it contributes greatly to a low on/off ratio. To overcome this limitation of graphene, graphene nanoribbon, bilayer graphene, and modified device architectures such as vertical tunneling transistor have been suggested. Although these methods have improved the on/off ratio to some extent, other desirable properties such as mobility and current density deteriorated. On the other hands, similar to the structure of graphene, 2D semiconductors are its isostructural counterparts based on the typical layer-structured transition metal dichalcogenides. Transition metal dichalcogenides (TMDs), a family of materials consisting of over 40 compounds with the generalized formula of  $\text{MX}_2$ , where M is a transition metal typically from groups 4-10, and X is a chalcogen such as S, Se or Te (Figure 1.1). Over several decades, bulk TMDs have been widely studied due to its disparate electronic structures. Layered TMDs have strong interlayer bonding and weak interlayer bonding. One layer of TMDs has three atomic structures in which the transition metal is sandwiched by two chalcogens. Because each individual layers are bonded with van der Waals forces, TMDs could be isolated by chemical and physical methods. Also, single-layer and multilayer TMDs have been synthesized by vapor deposition methods. The single-layer TMDs have unexpected properties compare to bulk TMDs due to the confinement of charge carriers in two dimensions and the absence of z-direction. Thus, it has shown potentials for wide-ranging applications such as catalyst, electronic and photonics.

|    |    |       |    |    |    |    |    |    |    |    |    |     |    |     |    |     |     |
|----|----|-------|----|----|----|----|----|----|----|----|----|-----|----|-----|----|-----|-----|
| H  |    |       |    |    |    |    |    |    |    |    |    |     |    |     |    |     | He  |
| Li | Be |       |    |    |    |    |    |    |    |    |    | B   | C  | N   | O  | F   | Ne  |
| Na | Mg | 3     | 4  | 5  | 6  | 7  | 8  | 9  | 10 | 11 | 12 | Al  | Si | P   | S  | Cl  | Ar  |
| K  | Ca | Sc    | Ti | V  | Cr | Mn | Fe | Co | Ni | Cu | Zn | Ga  | Ge | As  | Se | Br  | Kr  |
| Rb | Sr | Y     | Zr | Nb | Mo | Tc | Ru | Rh | Pd | Ag | Cd | In  | Sn | Sb  | Te | I   | Xe  |
| Cs | Ba | La-Lu | Hf | Ta | W  | Re | Os | Ir | Pt | Au | Hg | Tl  | Pb | Bi  | Po | At  | Rn  |
| Fr | Ra | Ac-Lr | Rf | Db | Sg | Bh | Hs | Mt | Ds | Rg | Cn | Uut | Fl | Uup | Lv | Uus | Uuo |

$MX_2$   
 M = Transition metal  
 X = Chalcogen

**Figure 1.1** The transition metals and the three chalcogen elements that predominantly crystallize in those layered structure are highlighted in the periodic table. Partial highlights for Co, Rh, Ir and Ni indicate that only some of the dichalcogenides from layered structures. For instances,  $NiS_2$  is found to have apyrite structure but  $NiTe_2$  is a layered compound.<sup>5</sup>

## 1.1 Characteristic of Two-Dimensional Transition Metal Dichalcogenides

Single-layer TMDs with lamellar structures similar to that of graphite have received significant attention because some of them are semiconductors with sizable bandgaps and are naturally abundant. In contrast, graphene with hexagonal lattice, TMDs generalized formula is  $\text{MX}_2$ , where M is a transition metal of groups 4-10 and X is a chalcogen. The TMDs offer opportunities for fundamental and technological research in a variety of fields including catalysis, energy storage, sensing and electronic devices such as field effect transistors (FET) and logic circuits. The properties of bulk TMDs are diverse. These have range from insulators such as  $\text{HfS}_2$ , semiconductors such as  $\text{MoS}_2$  and  $\text{WS}_2$ , semimetals such as  $\text{WTe}_2$  and  $\text{TiSe}_2$ , to true metals such as  $\text{NbS}_2$  and  $\text{VSe}_2$ . Isolation of these materials into single-layer or few-layer maintains their intrinsic properties, and leads to additional characteristics due to confinement effect. As a result, the chemistry of TMDs offer opportunities for going beyond graphene and opening up new fundamental and technology pathway for inorganic 2D materials. In particular, we focused the Molybdenum disulfide ( $\text{MoS}_2$ ) belonging to the group six family of TMDs is the most studied among TMDs, it has been widely used such as photocatalyst, photovoltaic, battery and etc.

### 1.1.1 Crystal Structure

The  $\text{MoS}_2$  has two types such as 2H and 3R-phases, both are trigonal prismatic coordination in nature.<sup>6</sup> The 2H-phase structures is shown in Figure 1.2a, it has two layers per unit cell which is AB type of stacking in the hexagonal (H) symmetry. In comparison with the 2H-phase, the 3R-phase has three layers per unit cell in the rhombohedral (R) symmetry.<sup>6</sup> Thermodynamically, because the 2H-phase is more stable than 3R-phase, the 2H-phase is dominant in nature. Also 3R-phase is transformed to 2H-phase by the heating.<sup>7</sup> The intralayer bonding is strong compare to interlayer bonding in all TMDs. The bulk 2H- $\text{MoS}_2$  does not have inversion symmetry as shown in Figure 1.2a. It is made up of van der Waals bonded S-Mo-S units. The bulk 2H- $\text{MoS}_2$  is hexagonal structure with space group  $P63/mmc$ , which is consistent with space group number 194.<sup>6</sup> Figure 1.2c shows single-layer 1T- $\text{MoS}_2$  and each S-Mo-S units are energetically stable. The single-layer  $\text{MoS}_2$  consist of three atomic structures in which the transition metal (Mo) is sandwiched by two chalcogens (S). Due to the weak interaction between the layers (strong interaction within the layers), shearing generate more easily and formation of 1T-phase crystal is possible. As we know it, transmission electron microscopy (TEM) is one of direct methods to investigate the surface morphology and crystal structure of 2D materials. By using TEM, single-layer and multilayer TMDs can be easily identified through diffraction patterns because they have different dimension and loss of six-fold symmetry.<sup>8</sup>

### 1.1.2 Electronic Structure

Similar to Si, bulk MoS<sub>2</sub> in nature has an indirect band gap of ~ 1.2 eV<sup>9-11</sup> with valence band maximum at  $\Gamma$  point and conduction band minimum in between the  $\Gamma$ -K direction in Figure 1.3a. As the bulk MoS<sub>2</sub> was reduced to single-layer, increasing indirect band gap was changed to direct band gap of ~1.9 eV at K-point. The electronic structure with the number of layers is shown in Figure 1.3. The direct band gap of single-layer MoS<sub>2</sub> was confirmed by photoluminescence spectroscopy<sup>9, 12</sup> and this phenomenon will be discussed later. The states near the indirect band gap of a few-layer MoS<sub>2</sub> have been shown<sup>13</sup>. The linear combination of *d* orbitals on Mo atoms and *p<sub>z</sub>* orbitals on S atoms consist indirect band gap of MoS<sub>2</sub>. The conduction band at K-point consists of only localized *d* orbitals on Mo atoms. The direct band gap is less influenced by indirect band gap on number of layers (or interlayer coupling) because Mo atoms are sandwiched by S atoms in single unit. As a result, the quantum confinement effect along the *z*-axis increases the indirect band gap.

### 1.1.3 Optical Property

The optical properties of MoS<sub>2</sub> had been experimentally studied.<sup>6, 14-16</sup> The absorption spectrum of MoS<sub>2</sub> was calculated. It shows two distinct peaks at 1.88 and 2.06 eV,<sup>17</sup> which were assumed to the direct transitions between a split valence band and the conduction band at the K-point of the Brillouin zone. The optical adsorption spectrum could be understood by excitonic effects due to a reduced electron screening.<sup>18-21</sup> The two prominent resonance features for in-plane polarization were indicated by electron energy loss spectroscopy (EELS).<sup>22, 23</sup>  $\pi$  plasmons are emerged below 10 eV and  $\pi + \sigma$  plasmons are emerged above 10 eV.<sup>21</sup> Due to the collective  $\pi - \pi^*$  transitions,  $\pi$  plasmons arise in MoS<sub>2</sub>, while  $\pi - \pi^*$  and  $\sigma - \sigma^*$  excitations result in  $\pi + \sigma$  plasmons.<sup>22, 24</sup> Totally, 18 valence electrons in MoS<sub>2</sub> and 12 electrons per molecule with the mixture of *s*, *p*, and *d* orbitals from the  $\sigma$  valence band and the remaining six electrons are in charge of the  $\pi$  plasmon band.<sup>23</sup> Whereas, the one prominent resonance features for out-of-plane polarization were indicated by EELS. It shows that  $\pi + \sigma$  plasmons excitation was emerged above 10 eV. The  $\pi + \sigma$  plasmons polarization are broad (both perpendicular and parallel). When MoS<sub>2</sub> is isolated to single-layer,  $\pi$  and  $\pi + \sigma$  plasmons are red-shifted in the energies.<sup>22</sup> Which are consistent with the experimental result.<sup>25</sup>

By the Photoluminescence (PL) study on MoS<sub>2</sub>,<sup>12</sup> The single-layer MoS<sub>2</sub> showed distinct emissions at ~670 and 627 nm emerged from the direct excitonic transitions at the Brillouin zone K-point, while bulk MoS<sub>2</sub> exhibited negligible PL as shown in Figure 1.4a. The spin-orbital splitting of valence band causes two peaks at different energy.<sup>12</sup> The PL intensity inversely depended on the thickness of MoS<sub>2</sub>, thus the single-layer MoS<sub>2</sub> exhibit the strongest PL intensity. Also, Raman scattering of MoS<sub>2</sub> has

been studied by Lee *et al.*<sup>26</sup> The  $E_{2g}$  mode of in-plane vibration and  $A_{1g}$  mode of out-of-plane vibrations were observed. The Raman characteristics, namely, the frequency, intensity, and width of the two peaks were found strongly influenced by the layer number. By the increasing number of layer, the blue shift of  $A_{1g}$  and the red shift of  $E_{2g}$  were exhibited as shown in Figure 1.4b, c. These shifted peaks were attributed to the Columbic interaction and possible stacking-induced change of the intralayer bonding.



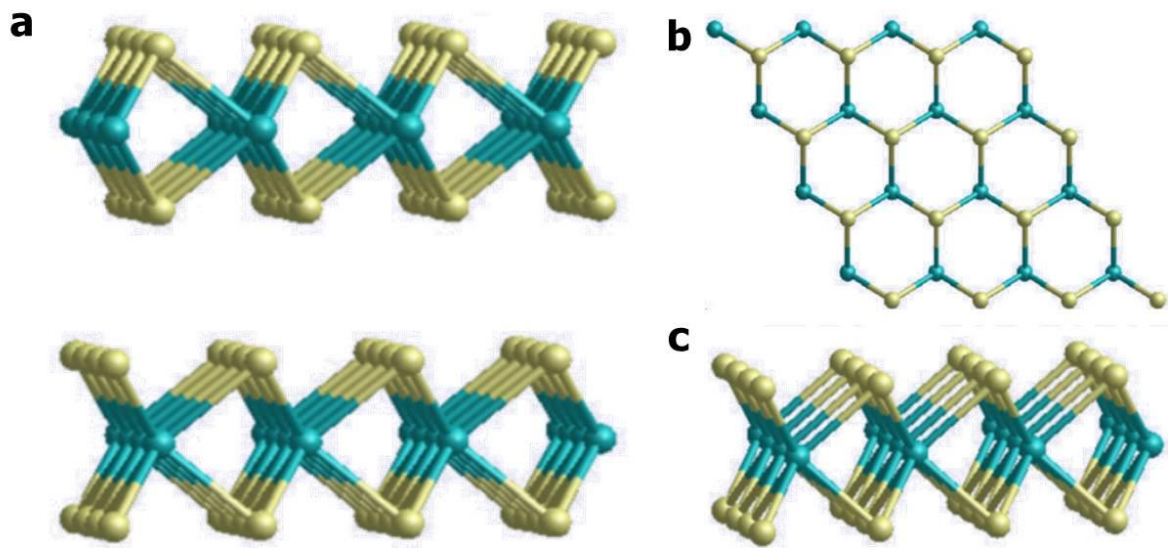


**Figure 1.2** (a) side view of bulk MoS<sub>2</sub> (van der Waals bonded MoS<sub>2</sub> units), (b) top view of both bulk MoS<sub>2</sub> and single-layer MoS<sub>2</sub>, (c) side view of single-layer MoS<sub>2</sub>.<sup>27</sup>

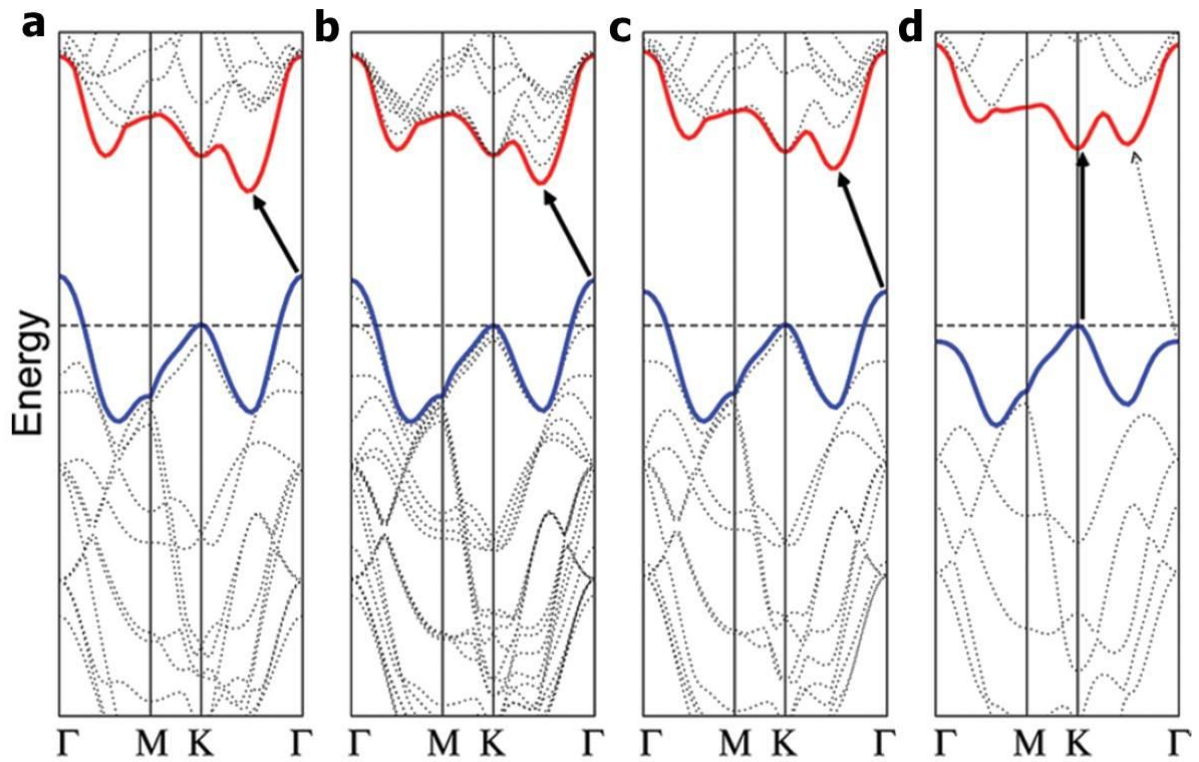


**Figure 1.3** Calculated electronic energy band-diagrams are shown for (a) bulk-MoS<sub>2</sub>, (b) 4-layer MoS<sub>2</sub>, (c) 2-layer MoS<sub>2</sub> and (d) single-layer MoS<sub>2</sub>. The solid arrow lines shown in Figure (a), (b) and (c) indicate the indirect transitions from valence band (at  $\Gamma$  point) to the conduction band minimum (along  $\Gamma$ -K direction), whereas in d it indicates the direct electronic transition at the K-point.<sup>12</sup>

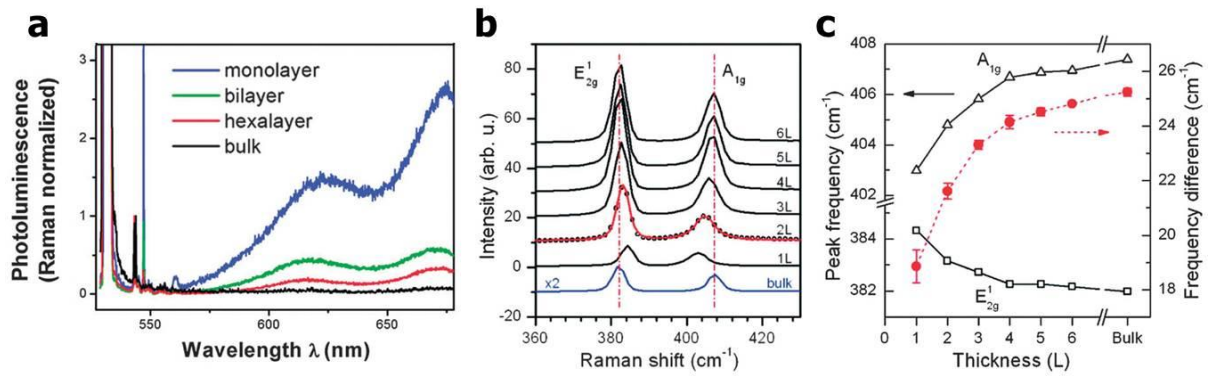


**Figure 1.4** (a) Photoluminescence spectra normalized by Raman intensity for MoS<sub>2</sub> layers with different thickness.<sup>12</sup> (b) Raman spectra of single-layer to bulk MoS<sub>2</sub>. The pump radiation was supplied by an Ar ion laser operating at a wavelength of 514.5 nm. The solid line for the 2-layer spectrum is a double Voigt fit by data (circles for 2-layer, solid lines for the rest).<sup>26</sup> (d) Frequencies of  $E_{2g}$  and  $A_{1g}$  Raman modes (left vertical axis) and their difference (right vertical axis) as a function of layer number.<sup>26</sup>

## 1.2 Isolation or Synthesis Method of Two-Dimensional Transition Metal Dichalcogenides

Graphene is the first 2D atomic crystal, and it is the thinnest substance ever obtained and the strongest material in the world. Graphene shows unusual condensed matter phenomena compared to graphite. Graphene was first discovered from graphite using “Scotch tape method” in 2004.<sup>1</sup> After that, many research groups have developed exfoliation methods and growth methods. Furthermore, other 2D materials which are transition metal dichalcogenides, hexagonal boron nitride were similarly researched and synthesized.

### 1.2.1 Mechanical Exfoliation

Bulk TMDs consist of stacked X-M-X layers. The X is chalcogen atom and the M is transition metal. While the intralayer bonding is strong within the layer, the interlayer bonding between layers is relative weak due to van der Waals interaction. It leads to mechanical cleavage of bulk TMDs. The mechanical exfoliate technique is used for obtaining single-layer graphene<sup>28, 29</sup> as well as various types of TMDs.<sup>28, 30-34</sup> Thin MoS<sub>2</sub> crystals were easily obtained by this technique, which repeatedly exfoliate the bulk crystals using adhesive tape, and subsequently transfer extracted crystals to substrate as shown in Figure 1.5. Also thickness of single-layer MoS<sub>2</sub> was confirmed by height profile of atomic force microscopy (AFM) as shown in Figure 1.5d.

### 1.2.2 Chemical Exfoliation

Another approach to produce mass production of 2D materials is chemical exfoliation. Chemical exfoliation of TMDs by direct sonication in common solution (dimethylformamide or N-methyl-2-pyrrolidone) has been used to graphene studies.<sup>35, 36</sup> Recently, this method was also used for fabricating single-layer and a few layers of TMDs, such as MoS<sub>2</sub>, WS<sub>2</sub>, TiS<sub>2</sub>, TaS<sub>2</sub>, ZrS<sub>2</sub>, NbSe<sub>2</sub><sup>37, 38</sup> as shown in Figure 1.6.

One of the most effective exfoliation methods is the hydration of TMD compounds by Li intercalation. For examples, single-layer MoS<sub>2</sub> was prepared by n-BuLi dissolved in hexane as the intercalation agent.<sup>39-41</sup> In this process, the formation of Li<sub>x</sub>XS<sub>2</sub> compound is important step and yield of single-layer sheets can be controlled. Also, Li intercalation method has an ability to access the metallic 1T-phase TMDs, which is induced by charge transfer from Li.<sup>42, 43</sup>

### 1.2.3 Chemical Vapor Deposition

Chemical vapor deposition (CVD) method of graphene has been studied for fabricating the large-area graphene. Along with the recent progress made in the research on graphene, synthesis of large-area MoS<sub>2</sub> using CVD has been demonstrated by several approaches.<sup>44-48</sup> Most of the current CVD research has focused on MoS<sub>2</sub>. Multi-layered MoS<sub>2</sub> was deposited by two-step thermolysis method as shown in Figure 1.7a, Coated in ammonium thiomolybdates [(NH<sub>4</sub>)<sub>2</sub>MoS<sub>4</sub>] on substrate was converted to MoS<sub>2</sub> sheets by thermal annealing at 500 °C and sulfurization at 1,000 °C by sulfur vapor.<sup>45</sup> As shown in Figure 1.7b, a different strategy that deposition of single-layer MoS<sub>2</sub> is based on the sulfurization of Mo metal thin films was reported.<sup>47</sup> As an alternative system in Figure 1.7c, the large-size single-layer MoS<sub>2</sub> flakes were synthesized by using the gas-phase reaction of MoO<sub>3</sub> and S powders.<sup>48</sup> Through the same system, a wafer-scale multilayer MoS<sub>2</sub> was synthesized by direct sulfurization of MoO<sub>3</sub> on sapphire substrate as shown in Figure 1.7d.<sup>49</sup> However, the large-area synthesis of single-layer TMDs using CVD systems remains a challenge.

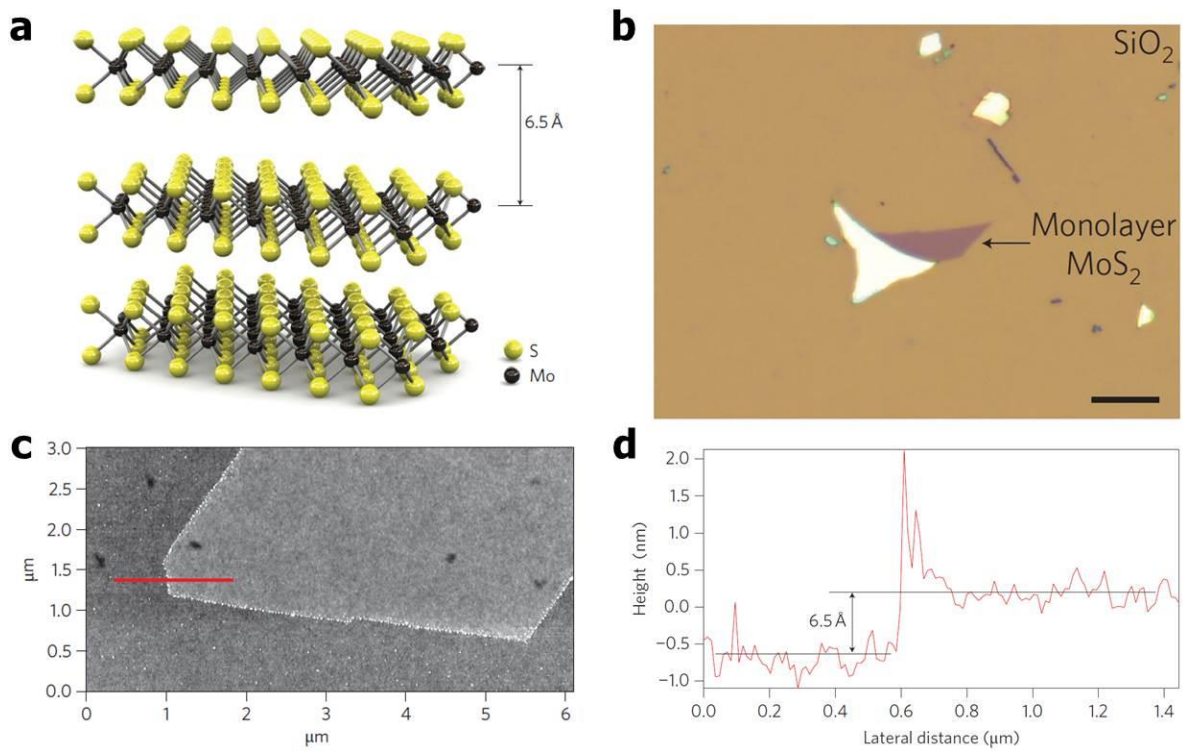


**Figure 1.5** Structure and microscopic image of single-layer MoS<sub>2</sub>. (a) Three-dimensional representation of the MoS<sub>2</sub>. (b) Optical image of single-layer MoS<sub>2</sub> deposited on SiO<sub>2</sub> substrate using scotch tape-based mechanical cleavage method. (c) AFM image of a single-layer MoS<sub>2</sub> on SiO<sub>2</sub> substrate. (d) Height profile along the red line in (c).<sup>34</sup>



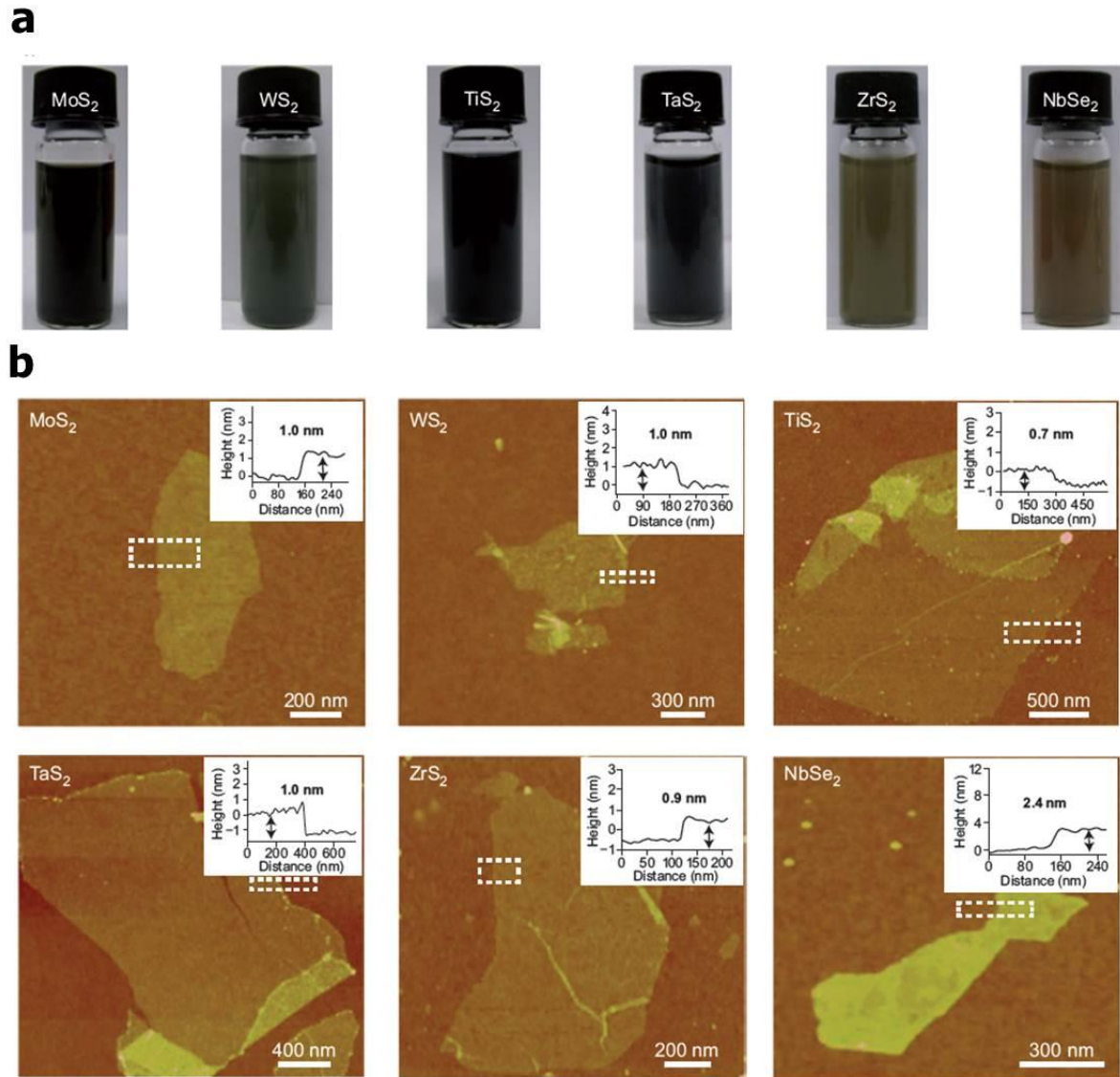


**Figure 1.6** (a) photographs of dispersed TMD nanosheets and (b) the AFM images corresponded with (a) on  $\text{SiO}_2$ . Insets exhibit thickness of nanosheets by height profiles.<sup>37, 38</sup>

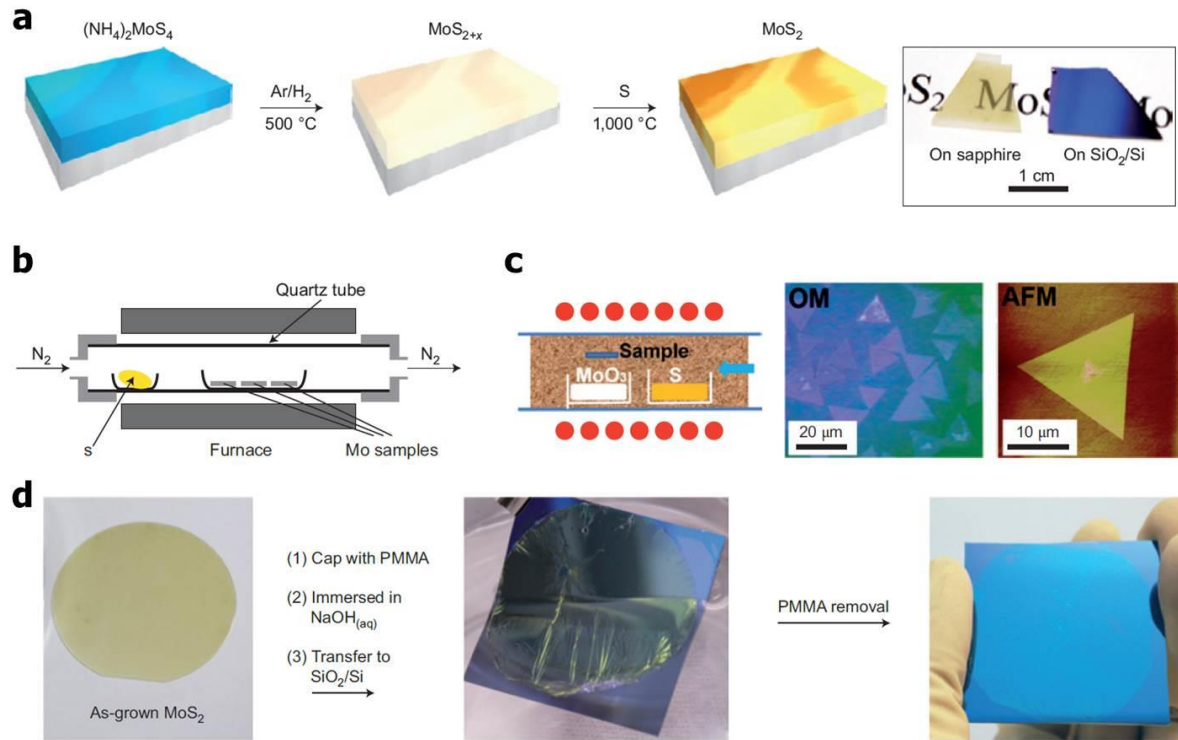


**Figure 1.7** Various chemical vapor deposition methods of TMDs. (a) Schematic description of two-step thermolysis, and the obtained MoS<sub>2</sub> films on sapphire and silica substrate.<sup>45</sup> (b) Schematic CVD system of synthesizing single to few-layer MoS<sub>2</sub> by sulfurization of Mo metal thin film.<sup>47</sup> (c) Growth system of single-layer MoS<sub>2</sub> using MoO<sub>3</sub> and S powders by a gas-phase reaction.<sup>48</sup> (d) Wafer-scale synthesis of a few-layer MoS<sub>2</sub> films through direct sulfurization of MoO<sub>3</sub> films. It transfers onto arbitrary substrate.<sup>49</sup>



### 1.3 Functionalization of Two-Dimensional Materials

Surface modification is ways to modulating the properties of 2D-materials such as graphene, h-BN and TMDs. There are various methods for modifying the intrinsic properties in graphene studies. However, surface modulating methods of the TMDs remain a challenge in this area.

#### 1.3.1 Covalent Functionalization

Chemical functionalization of two-dimensional transition metal dichalcogenides (TMDs) nanosheets ( $\text{MoS}_2$ ,  $\text{WS}_2$ ,  $\text{MoSe}_2$ ,  $\text{WSe}_2$ , etc.) leads to significant changes in their intrinsic properties and is important to improve the solubility in common solvents. Covalently attached functional groups at defect sites usually led to electron transfer from functional group to TMD.<sup>50, 51</sup> Single-layer  $\text{MoS}_2$  had been described as perfect crystal structure. Along with, it has outstanding property for catalysis.<sup>52</sup> Tuxen *et al.* first found the functionalization of single-layer  $\text{MoS}_2$  by scanning tunneling microscopy.<sup>53</sup> They demonstrated that the dibenzothiophene (DBT) could be covalently attached on single-layer  $\text{MoS}_2$  nanoclusters. It showed a strong bonding between the inorganic molecules and organic functional group by the thermal stability and shorter Mo-S distance. Chou *et al.* demonstrate the chemical functionalization of  $\text{MoS}_2$  with thiol ligands.<sup>51</sup> The functionalized  $\text{MoS}_2$  by thiol group exhibited remarkable colloidal stability in water. Moreover, modified surface charge from negative to positive prevented the aggregation and precipitation of mixed materials in acidic medium solution. Zhou *et al.* reported surface modification of *n*-BuLi exfoliated  $\text{MoS}_2$ .<sup>54</sup> The purpose of this reaction is modifying its physical properties. If the anchored ligands carry additional functional groups, the  $\text{MoS}_2$  can be changed to chemically reactive state. This makes the novel materials to useful building blocks in multi-step synthetic process.  $\text{Li}_x\text{MoS}_2$  powder reacted with Thioglycerol (TG), cysteine and mercaptopropionic (MPA). And produced hydroxyl, carboxyl, amino groups enhance the dispersibility in water.

Also, covalent functionalization is also used to modulate the optical and electrical properties. Voiry *et al.* showed surface functionalization of 1T-TMDs by organic molecules such as  $-\text{CH}_3$  and  $-\text{CH}_2\text{CONH}_2$ .<sup>55</sup> The functionalized 1T-phase TMD exhibited modified electrical properties, which is semiconducting property from metallic of pristine 1T- $\text{MoS}_2$  as shown in Figure 1.8b. Functionalization gives it strong and tunable photoluminescence as shown in Figure 1.8c. However, these changes such as optical and physical properties have not been clearly understood.

### 1.3.2 Functionalization with Nanoparticles

For using optoelectronic applications of TMDs, modulating the electronic properties is important. It can be modified by mobile charge concentrations. And it is known for that the incorporation of nanoparticles (NPs) of noble metals is an effective way to doping 2D TMD materials. Doping effect in TMDs was investigated by Sarkar *et al.* they used noble metal such as Au, Ag, Pd, Pt. These NPs caused p-type doping of MoS<sub>2</sub>. In particular, Pt NPs can cause twice higher p-type effect in comparison with commonly used Au NPs.<sup>56,57</sup> Due to their high surface to volume ratio and sensitivity, nanoparticle functionalized TMDs are highly advantageous for gas sensing.<sup>58</sup>

### 1.3.3 Hydrogenation

Surface hydrogenation has dramatically changed the electronic structure of graphene. Covalently attached hydrogen on graphene modified from sp<sup>2</sup> bonding of carbons to sp<sup>3</sup> of hybridization state. Thus, the delocalized electron was broken in graphene. Sofo *et al.* theoretically explained the existence of hydrogenated graphene.<sup>59</sup> This theory was realized by experiment of hydrogenated graphene.<sup>60</sup> They opened band gap of graphene by hydrogenation using exposure to cold hydrogen plasma. Also, the degree of hydrogenation was controlled by partially hydrogenated graphene.<sup>61</sup>

Chemically attached hydrogen atoms also carry a considerable relationship with TMD materials. For examples, exfoliated TMD nanosheets show extraordinary hydrogen evolution reaction (HER) catalytic activity. However, effects of attached hydrogen atoms on TMD nanosheets are rarely investigated in detail in electronic and optical properties experimentally. Tang *et al.* investigated the potential of hydrogenation of monolayer 1T-MoS<sub>2</sub> in tuning its electronic properties by first-principles computational study.<sup>62</sup> They explained that the affinity of attaching hydrogen is different in the 2H and 1T phase. At high coverage of hydrogen, 1T-MoS<sub>2</sub> was energetically more stable than 2H-MoS<sub>2</sub> due to its metallic character. More interestingly, the band gap of 1T-MoS<sub>2</sub> can be modulated by degree of hydrogen coverage as shown in Figure 1.9a. He *et al.* investigated the electronic and magnetic properties of hydrogen attached single-layer MoS<sub>2</sub> by DFT calculation.<sup>63</sup> The theoretical predictions showed that the H and N atoms attached on S atoms lead to n- and p-type semiconducting behaviors, respectively. And hydrogen lead to long-range antiferromagnetic coupling in single-layer MoSe<sub>2</sub>, WS<sub>2</sub> and MoTe<sub>2</sub>.<sup>64</sup> Zhang *et al.* predicted hydrogenation of 2H-MoS<sub>2</sub> by first-principles study.<sup>65</sup> They demonstrated S-H bonding is more favorable than Mo-H bonding and hydrogenation of MoS<sub>2</sub> is energetically stable reaction. As a simulation, the band gap can be modulated by degree of hydrogenation.

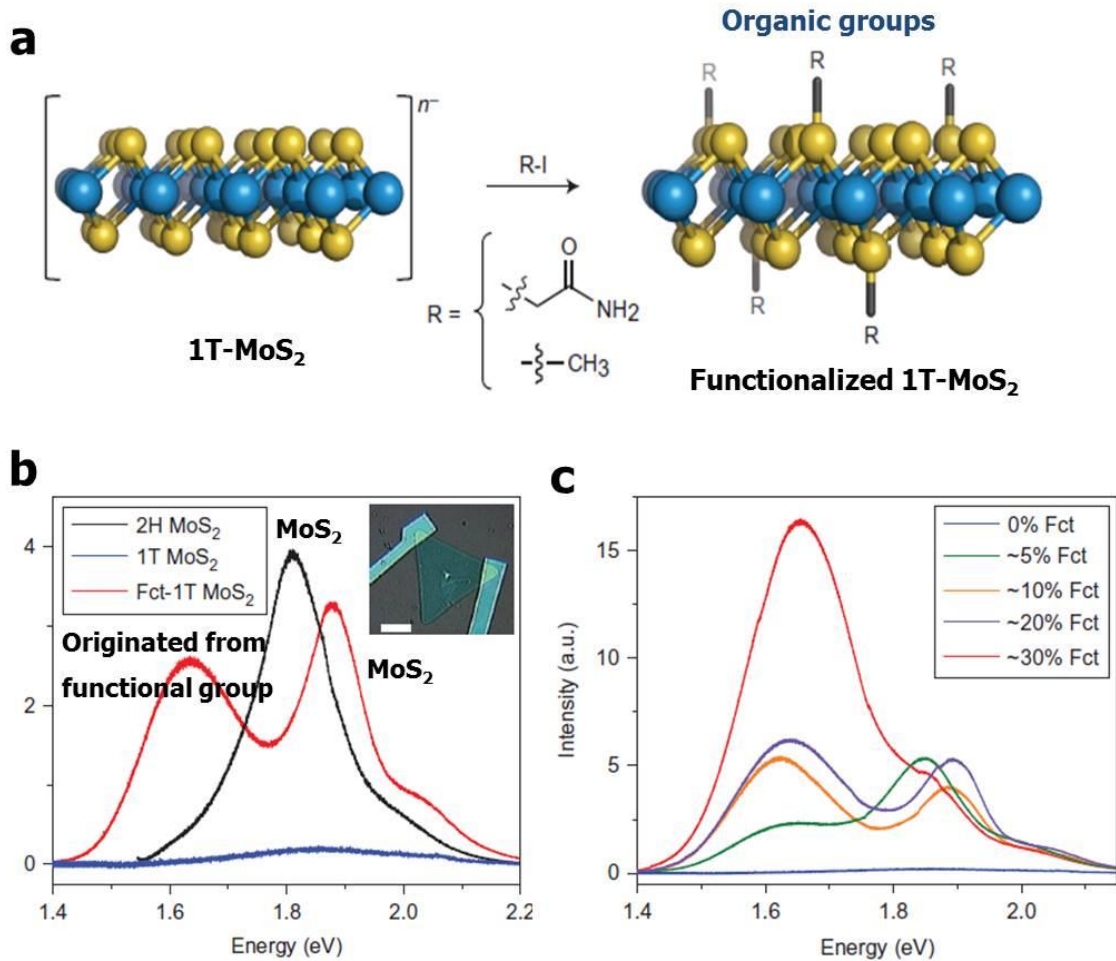


**Figure 1.8** (a) Scheme of the functionalization strategy (b) Photoluminescence spectra from single-layer 2H-MoS<sub>2</sub> synthesized by CVD, from the metallic 1T-MoS<sub>2</sub> and from the functionalized 1T-MoS<sub>2</sub>. Inset is a CVD-grown single-layer MoS<sub>2</sub> on which the photoluminescence spectra were measured. (c) Modulated photoluminescence with increasing degree of functionalization.<sup>55</sup>

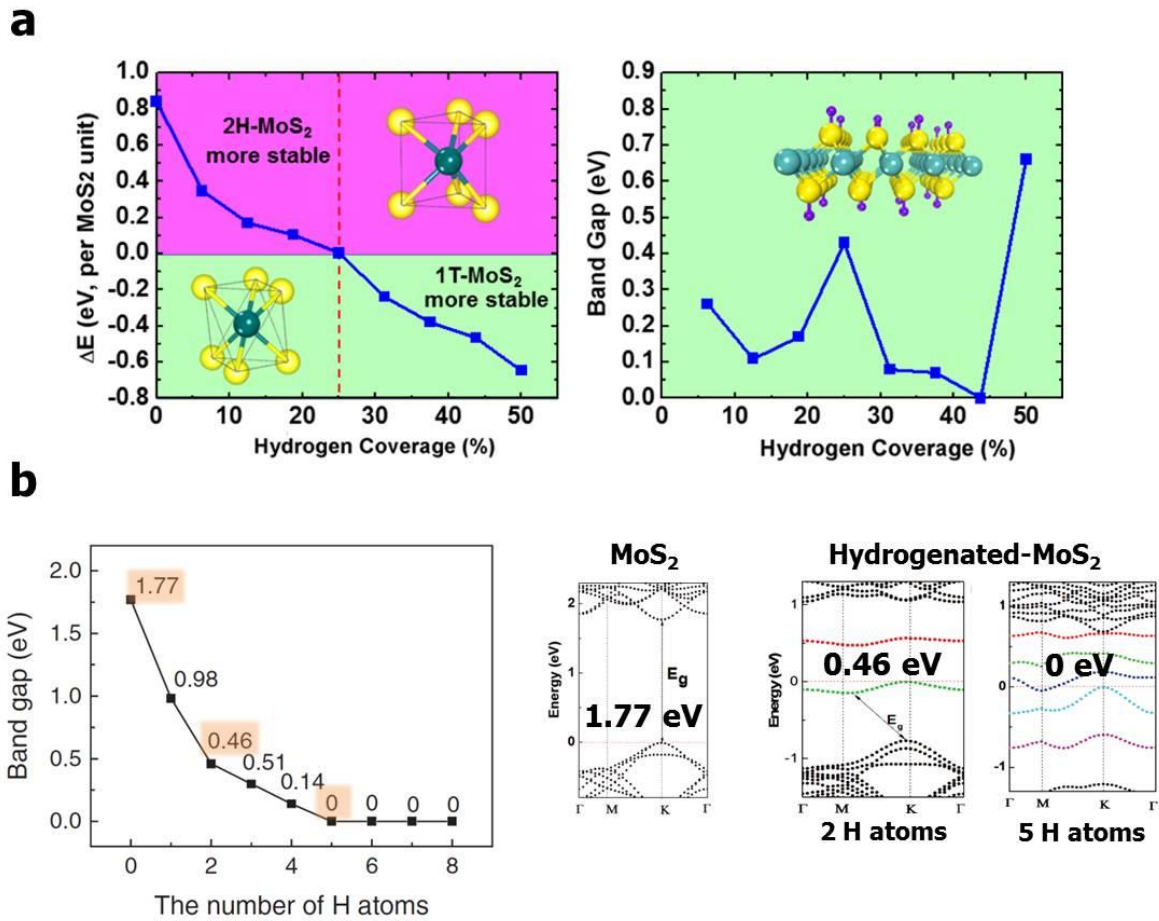


**Figure 1.9** (a) Difference of energy between 1T and 2H-MoS<sub>2</sub> as a function of the attached hydrogen coverage (on S atoms) and calculated band gap of 1T-MoS<sub>2</sub> by different hydrogen coverage.<sup>62</sup> (b) Calculated band gap of 2H-MoS<sub>2</sub> as a function of the number of attached hydrogen atoms. And band structure of pristine 2H-MoS<sub>2</sub> and hydrogenated MoS<sub>2</sub>.<sup>65</sup>

## 2. Experimental section

### 2.1 Synthesis of Monolayer MoSe<sub>2</sub>

Single-layer MoSe<sub>2</sub> was synthesized by a simple atmosphere pressure (AP) CVD method. Selenium powder (100 mg) and molybdenum oxide (MoO<sub>3</sub>) (60 mg) powder were used as Se and Mo precursor, respectively. In a typical CVD growth, an alumina boat containing 60 mg of MoO<sub>3</sub> powder located at the centre of the heating zone and another alumina boat with 100 mg of Se powder located upstream outside of the furnace was increase the temperature to 250 °C by using heating coil. The sapphire substrate was located downstream 20-40 cm away from the MoO<sub>3</sub> powders in the furnace. The furnace temperature was raised up to 700 °C for 34 min (600 °C for 25 min and 700 °C for 10 min) gradationally. After that, to grow the MoSe<sub>2</sub> triangle domains, the temperature was held at 700 °C for 45 min. After growth, the furnace was left to cool unassisted. During growth process, 75 standard cubic centimeters per minutes (sccm) mixture of argon and hydrogen gases (7.7 % hydrogen) was used for carrier gases.

### 2.2 Characterization of Single-layer MoSe<sub>2</sub>

The surface morphology of the samples was characterized by optical microscopy (Axio Scope.A1, Carl Zeiss), SEM (S-4800, Hitachi), and AFM (Dimension 3100, Veeco). Raman and Photoluminescence spectra were measured using a micro Raman spectrometer (Alpha 300s, WITec) equipped with a 532 nm laser. X-ray photoelectron spectra (K-Alpha, Thermo Fisher) were measured to identify MoSe<sub>2</sub> molybdenum and selenium. The electrical characteristics of the MoSe<sub>2</sub>-based field effect transistors were determined using the four-point probe technique.

### 2.3 Hydrogenation of MoSe<sub>2</sub>

The samples were exposed to radio frequency plasma generator. The plasma power was 20 W and 5 sccm of hydrogen gases were used in vacuum (1 mbar). Reaction time was separated from 42 to 168 seconds to control degree of hydrogenation.

## 2.4 Fabrication of MoSe<sub>2</sub> Field Effect Transistor

After the synthesis of MoSe<sub>2</sub> on sapphire, the MoSe<sub>2</sub>/sapphire was covered with PMMA (AR-P 671.04, Allresist) by spin coating (4,000 rpm for 60 sec). The PMMA coated MoSe<sub>2</sub> were peeled off from sapphire during etching of sapphire by the diluted HF solution (10 %). The PMMA/MoSe<sub>2</sub> was washed with fresh DI water several times, finally leaving the PMMA/MoSe<sub>2</sub> floating on the surface of the water and ready for transfer to the SiO<sub>2</sub>/Si substrate.

After transferred MoSe<sub>2</sub> to SiO<sub>2</sub>, back-gate field effect transistor was fabricated by electron beam lithography (Nanobeam nB4, NBL) using a positive electron beam resist (AR-P 671.04, Allresist), and metal deposition (Ti (3 nm) / Au (35 nm)), followed by a lift off process. Au and Ti were used for electrodes and adhesion layer, respectively.

## 3. Result and Discussion

### 3.1 Surface Characterization Single-layer Pristine MoSe<sub>2</sub> and Hydrogenated MoSe<sub>2</sub>

MoSe<sub>2</sub> is an interesting 2D optoelectronic material due to its narrow and direct optical band gap. It was synthesized by CVD method and characterized with Raman spectroscopy and electron microscopy. MoSe<sub>2</sub> was grown by using MoO<sub>3</sub> and selenium powder on a clean sapphire substrate as shown in Figure 2.1a. During growth process, mixture of argon and hydrogen gases (7.7 % hydrogen) was used for carrier gases. As reported in the WSe<sub>2</sub> system<sup>66</sup> without hydrogen gas, MoSe<sub>2</sub> deposition does not occur. After growth at 700 °C for 45 min, MoSe<sub>2</sub> flake was deposited on sapphire substrate as shown in Figure 2.1b. As shown in AFM and SEM images, (Figure 2.1c and d, respectively) most of the MoSe<sub>2</sub> flakes have uniform surface morphology and size of the triangles ranges from a few microns to 10 μm. The thickness was 0.79 nm as measured by AFM (Figure 2.1e). Therefore, it was perfectly single-layer MoSe<sub>2</sub> which is consistent with the as reported in the MoSe<sub>2</sub> system.<sup>67</sup> As-grown MoSe<sub>2</sub> flakes were further characterized by Raman, PL and UV-visible spectroscopy. The triangular MoSe<sub>2</sub> flake was measured with Raman and PL using a 532 nm excitation laser. There are two typical peaks in the Raman spectrum. A sharp peak at 240 cm<sup>-1</sup> is A<sub>1g</sub> mode (out-of-plane vibration of Se atoms) and a relatively broad peak at 286 cm<sup>-1</sup> is E<sub>2g</sub> mode of MoSe<sub>2</sub> (in-plane vibration of Mo and Se atoms).<sup>68, 69</sup> It is corresponding to a Raman shift of A<sub>1g</sub> and E<sub>2g</sub> mode (Figure 2.2a) in excellent agreement with the previously reported for single-layer MoSe<sub>2</sub>.<sup>67</sup> Electronic structures of MoSe<sub>2</sub> are different with its thickness.<sup>44, 70</sup> Our CVD-grown MoSe<sub>2</sub> was confirmed by PL using 532 nm laser. Figure 2.2b shows the definite single emission peak at 1.56 eV which is consistent

with the previously reported papers.<sup>67, 71, 72</sup> It can be ascribed to the direct band gap at the K high symmetry point of the Brillouin zone.<sup>73</sup> Also, through the observation of the PL map at 1.56 eV, it shows uniformity of MoSe<sub>2</sub> flakes in inset of Figure 2.2b. The UV-visible spectrum shows strong PL emission from the single-layer MoSe<sub>2</sub>. Two main peaks appear at 790 nm (1.57 eV) and 700 nm (1.77 eV) which are A and B excitons, respectively, as shown in Figure 2.2c. Both A and B exciton energies are in agreement with previously reported experimental results.<sup>74</sup> The strong spin-orbit interaction causes the spin splitting energy of A and B excitons by theoretical calculations.<sup>72, 75</sup>

After initial characterization, the MoSe<sub>2</sub> on sapphire (or SiO<sub>2</sub>) were exposed to radio frequency plasma generator. The plasma power was 20 W and 5 sccm of hydrogen gases were used in vacuum (1 mbar). Reaction time was separated from 42 to 168 seconds to control degree of hydrogenation. The required saturation time of hydrogen plasma treatment was 168 seconds in measured characteristics. However, because the hydrogen was known to etch the surface in 2D materials such as graphene<sup>76-80</sup>, hexagonal boron nitride<sup>81-83</sup>, we checked the unchanged surface after hydrogen plasma treatment. After hydrogen plasma treatment for 10 min, not only uniform surface morphology but also thickness was virtually unchanged as shown in Figure 2.3. However, distinct change induced by the hydrogen plasma in PL map was observed on the same MoSe<sub>2</sub> flake in inset of Figure 2.3a and b.



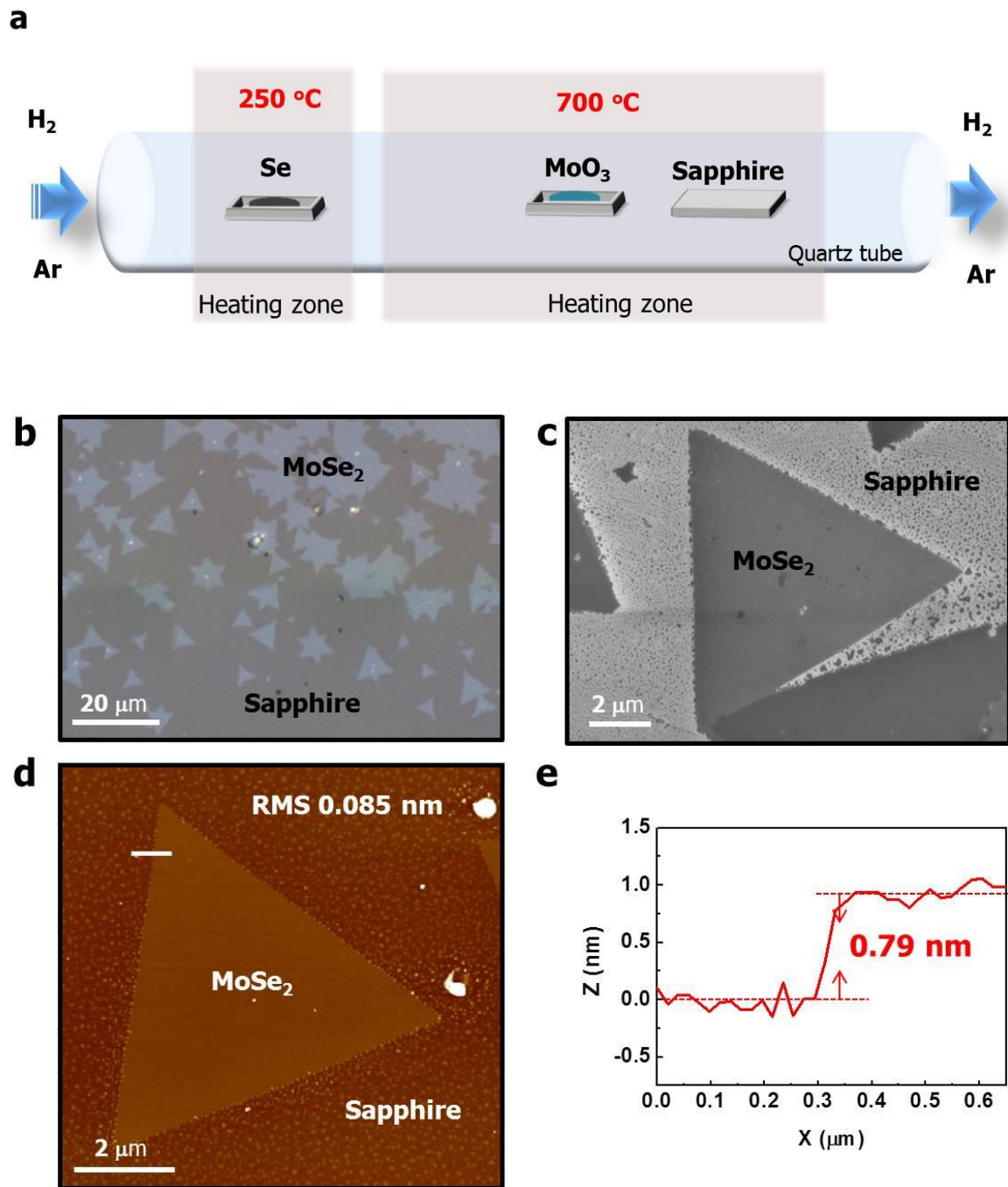


**Figure 2.1** (a) Schematic of the growth setup for synthesizing  $MoSe_2$ . Initial microscopic characterization of single-layer  $MoSe_2$  flakes. (b) Optical image and (c) SEM image of single-layer  $MoSe_2$ . (d) AFM height topography of single-layer  $MoSe_2$  on sapphire. (Inset) Height profile of write line marked in (d).



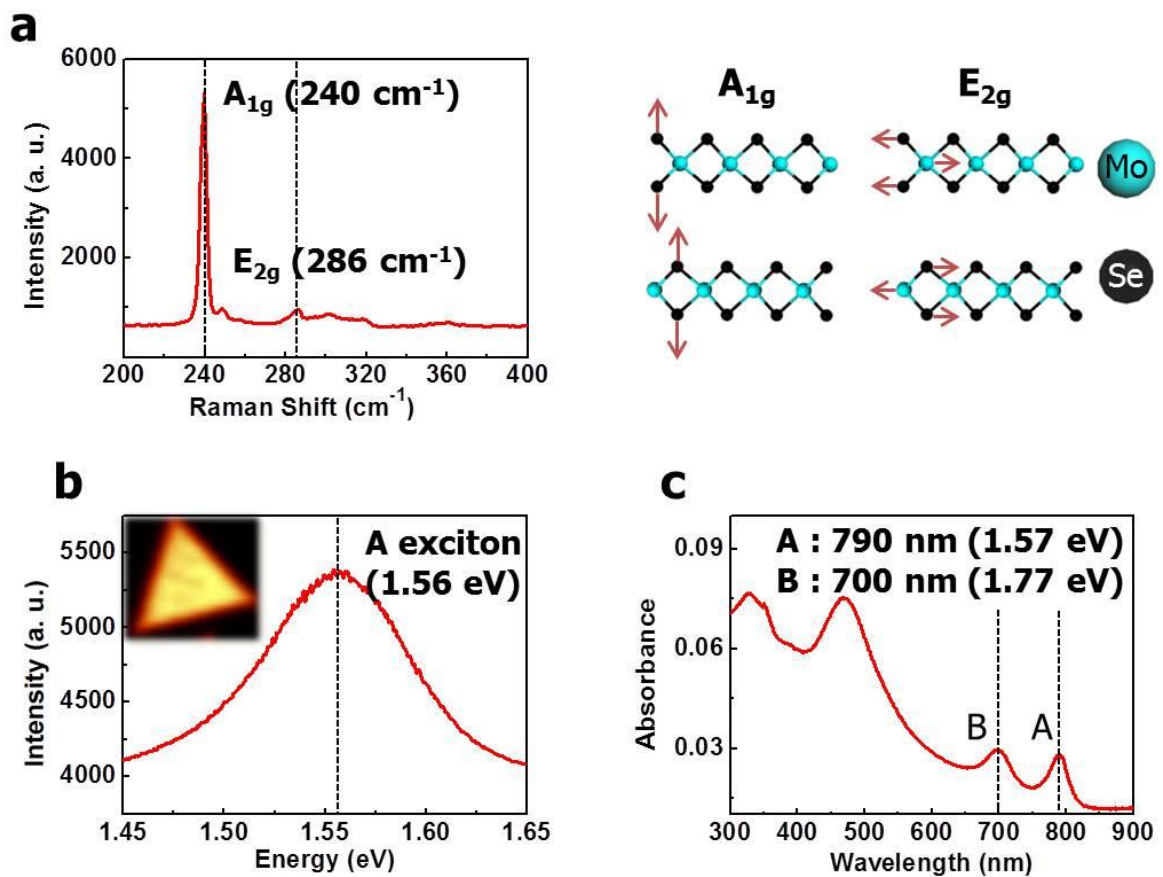


**Figure 2.2** Initial spectroscopic characterization of single-layer  $\text{MoSe}_2$  flakes on sapphire. (a) Raman spectrum and vibration direction of  $A_{1g}$  and  $E_{2g}$  mode. (b) PL spectrum. (Inset) PL mapping. (c) UV-vis-NIR spectrum of CVD grown  $\text{MoSe}_2$ .

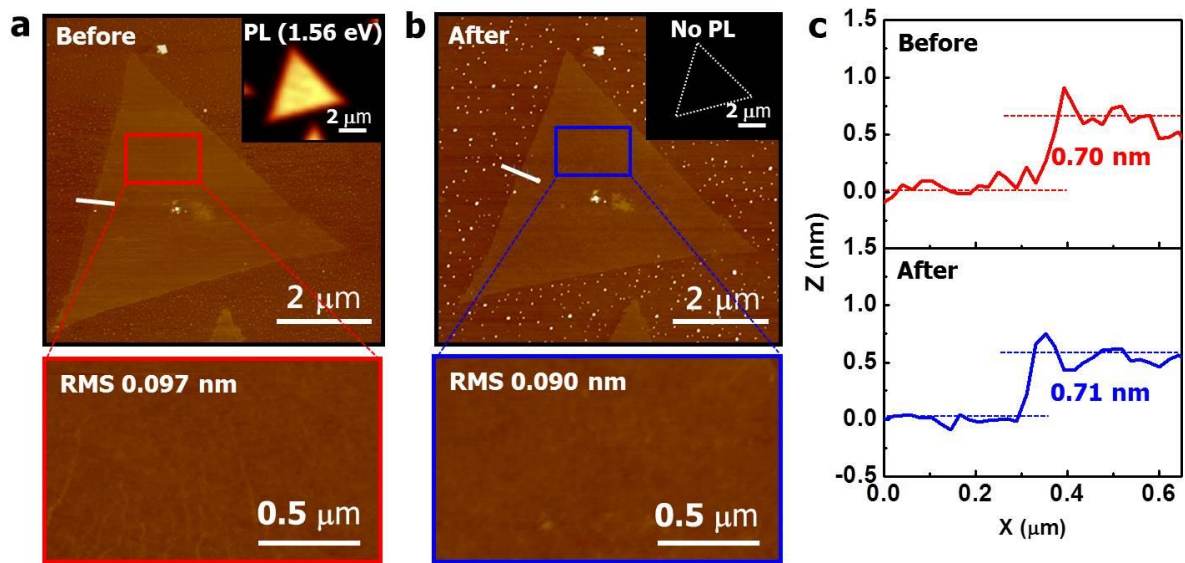


**Figure 2.3** AFM height topography of single-layer MoSe<sub>2</sub> on sapphire (a) before and (b) after 10 minutes hydrogenation. Inset : homogeneous PL peak of single-layer MoSe<sub>2</sub> (a) before and (b) after hydrogenation. (c) Height profile of (a) and (b). MoSe<sub>2</sub> flakes remained intact after H<sub>2</sub> plasma treatment.

### 3.2 Photoluminescence and Raman of Hydrogenated MoSe<sub>2</sub>

To investigate the change of PL, the arbitrarily selected MoSe<sub>2</sub> flake was used for time dependence experiment. Figure 2.4a shows intensity of PL get lower with increasing exposure time. A comparison of PL spectra result for pristine MoSe<sub>2</sub> and fully hydrogenated MoSe<sub>2</sub> gives distinct change by different reaction time as shown in Figure 2.4b. After reaction for 42 seconds, a red shift from 1.56 to 1.51 eV is observed. It might be possible that the origin of peak shift is additional energy state which was originated from attached hydrogen on surface of MoSe<sub>2</sub>. In theoretical study of hydrogenated MoS<sub>2</sub>, because unoccupied impurity states were caused on pristine MoS<sub>2</sub> by chemisorbed hydrogen atoms, semiconducting MoS<sub>2</sub> which has direct band gap of 1.77 eV is converted into an indirect semiconductor with the reduced band gap after adsorption of hydrogen atoms on the surface.<sup>65</sup> After 42 seconds of hydrogenation, the structural change was induced by additionally attached hydrogen, thus PL was removed. From the comparing the intensity of PL at different time, degree of change was different by position (Figure 2.4c, e). Faded out of PL was only in edge site at 84 seconds. Therefore, we could conclude that the hydrogenation initialized at edge area. The same phenomenon was found by UV-visible spectroscopy. Both A and B exciton peaks from pristine MoSe<sub>2</sub> were declined by hydrogenation (Figure 2.4d).

Through Raman spectroscopy analysis, the changes caused by hydrogenation have been observed in Figure 2.5. Hydrogenated MoSe<sub>2</sub> with different reaction time shows decrease in intensity and shift of peak position of A<sub>1g</sub> mode vibration from 240 to 234 cm<sup>-1</sup> as shown in Figure 2.5a. It might be possible that the decrease of intensity was from reduced crystallinity of pristine MoSe<sub>2</sub> and shift of peak position could be originated by charge transfer from attached hydrogen atoms. The new peak in hydrogenated MoSe<sub>2</sub> is observed at 272 cm<sup>-1</sup>, which is increased by the reaction time as shown in Figure 2.5b. However, it has been still unknown. The E<sub>2g</sub> mode, in-plane vibration of Mo and Se atoms, does not change during hydrogenation as shown in Figure 2.5b. A related phenomenon of changed A<sub>1g</sub> mode has been reported by Voiry *et al.* for chemically functionalized 1T-MoS<sub>2</sub>, 1T-WSe<sub>2</sub>, and 1T-MoSe<sub>2</sub> by organic groups.<sup>55</sup> In their case, only A<sub>1g</sub> peak of TMDs was changed by functional groups. The explanation given by Voiry is that the perturbation of the vibration from the chalcogen atoms such as S and Se caused by the anchorage of the functional groups.

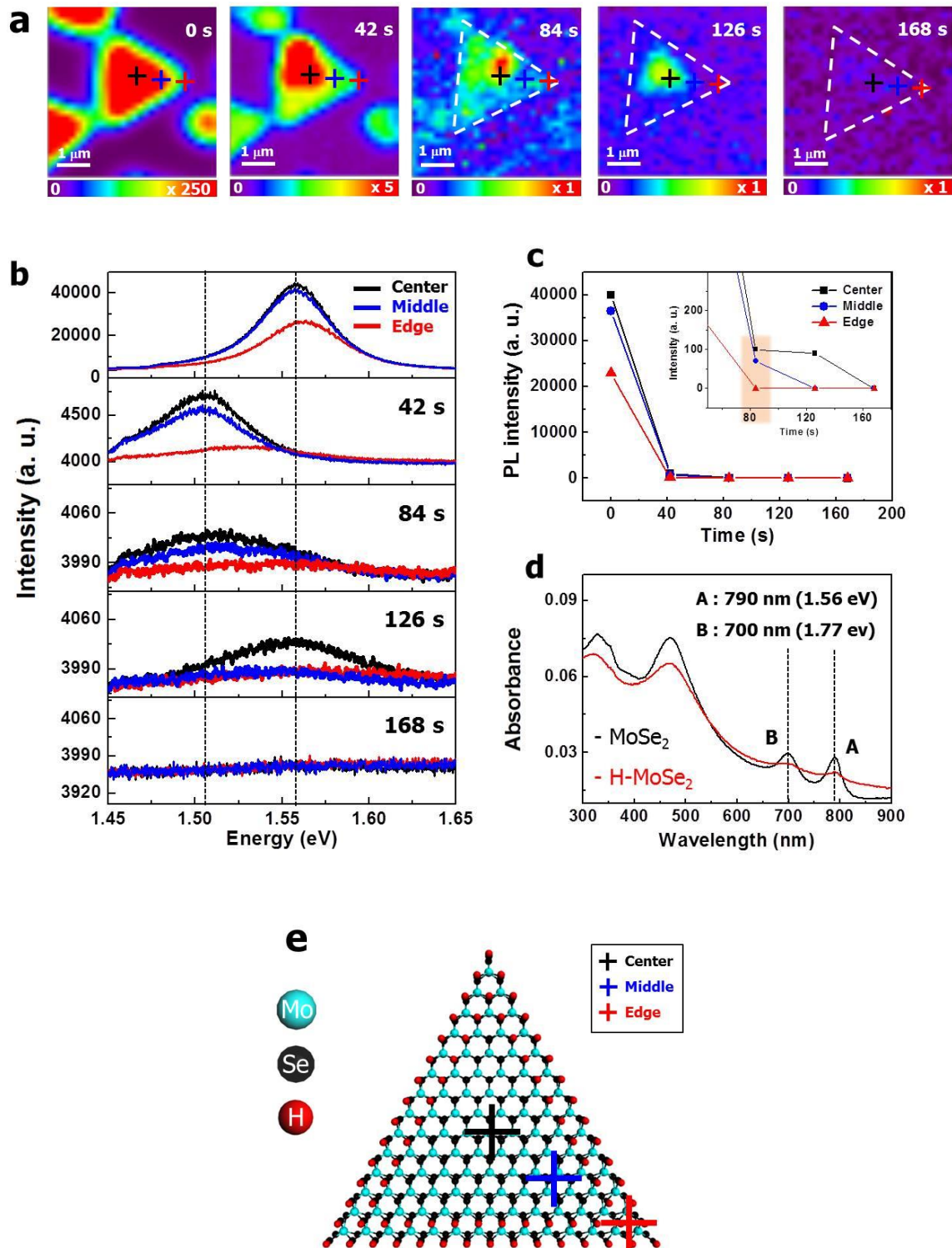


**Figure 2.4** PL characterization of hydrogenated MoSe<sub>2</sub>. (a) PL mapping images and (b) PL spectra at center, middle and edge sites of MoSe<sub>2</sub> flakes with different times. (c) PL intensity-time curves at different position. Inset spectra show magnified curves of (c) from 84 seconds to 168 seconds. (d) UV-vis-NIR spectra of before and after hydrogenated MoSe<sub>2</sub> (black line : before, red line : after). (e) Schematic of hydrogenated MoSe<sub>2</sub> at 84 seconds.

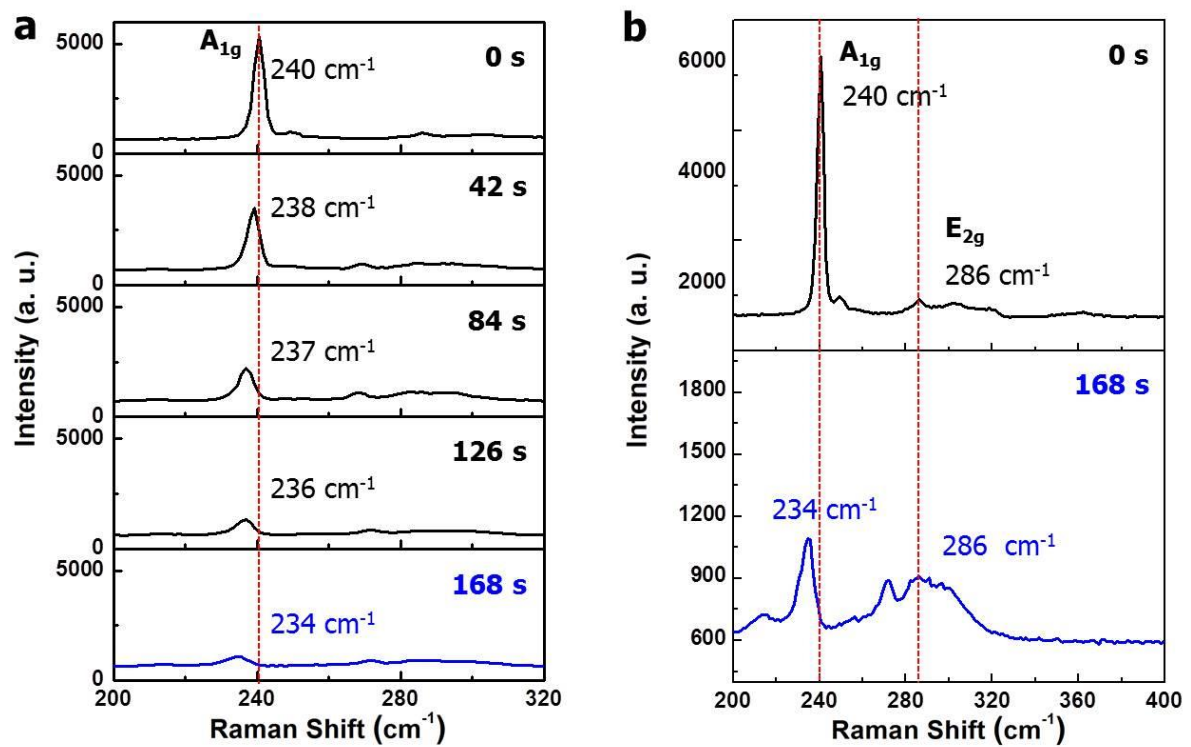
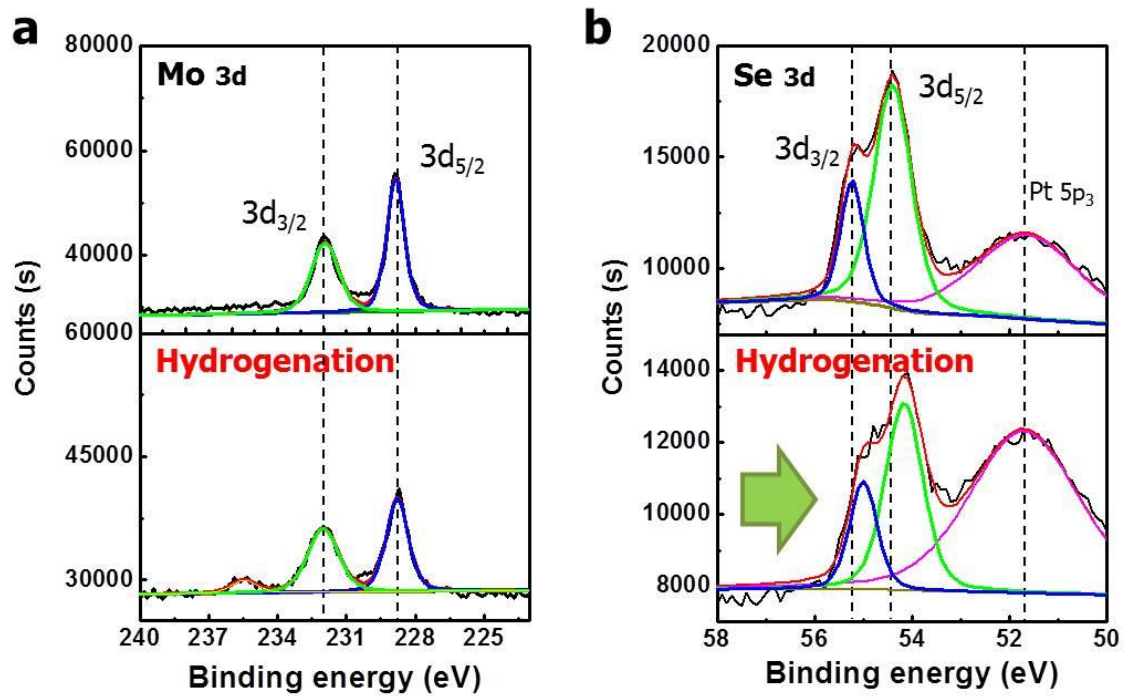


**Figure 2.5** (a) Raman spectra of hydrogenated MoSe<sub>2</sub> with different reaction time. (b) Raman spectra of before and after hydrogenated MoSe<sub>2</sub> for 168 seconds.

### 3.3 Analysis of X-ray Photoelectron Spectrum on Hydrogenated MoSe<sub>2</sub>

The binding energy in the CVD grown single-layer MoSe<sub>2</sub> was indicated by X-ray photoelectron spectroscopy (XPS). To suppress the charging effect and noise from substrate, as grown single-layer MoSe<sub>2</sub> flakes were transferred to Pt substrate. Furthermore, noble metal is useful to discern small change of binding position as a standard point. The upper spectra of Figure 2.6 provide bonding information of Mo 3d and Se 3d in the MoSe<sub>2</sub>. The core level peaks of Mo 3d<sub>3/2</sub> and 3d<sub>5/2</sub> are located at 231.90 and 228.60 eV (upper spectrum of Figure 2.6a), respectively. And the peak of Se around 54.00 eV can be divided into Se 3d<sub>3/2</sub> and Se 3d<sub>5/2</sub> with peak positions at 55.23 and 54.39 eV (upper spectrum of Figure 2.6b), respectively.<sup>66</sup> These measured values are in agreement with other MoSe<sub>2</sub> systems.<sup>67, 84, 85</sup>. After hydrogenation for more than 168 seconds, it was found that the only change of binding energy to lower energy state on Se 3d. However, binding energies of Mo 3d<sub>3/2</sub> and Mo 3d<sub>5/2</sub> were not change as shown in down spectra of Figure 2.6. This implies hydrogen is bonded with Se rather than Mo. Moving to lower energy was related with changed work function. Theoretically, attached hydrogen atoms donate its electrons to the surface, which gives rise to the formation of outward pointing surface dipole moment from the surface to vacuum in MoS<sub>2</sub> system.<sup>65</sup> This causes decrease of work function. Moreover, because electron negativity of Se (2.1) is lower than hydrogen (2.4), moving to lower energy was reasonable. Also, it can be evidenced that the bonding of Mo and Se does not broken by XPS results.





**Table**

|                     | Mo 3d <sub>3/2</sub> | Mo 3d <sub>5/2</sub> | Se 3d <sub>3/2</sub> | Se 3d <sub>5/2</sub> |
|---------------------|----------------------|----------------------|----------------------|----------------------|
| MoSe <sub>2</sub>   | 231.90               | 228.60               | 55.23                | 54.39                |
| H-MoSe <sub>2</sub> | 231.90               | 228.62               | 55.00                | 54.17                |

\* Standard : Pt 5p<sub>3/2</sub> (51.70 eV)

**Figure 2.6** X-ray photoelectron spectra of single-layer MoSe<sub>2</sub> on platinum substrate before and after hydrogenation (a) XPS spectra of Mo 3d and (b) XPS spectra of Se 3d. Table is comparison of the binding energy of Mo 3d and Se 3d with hydrogenated Mo 3d and Se 3d.

### 3.4 Electron Transport Property of Hydrogenated MoSe<sub>2</sub>

To fabricate back-gate FET device, as grown MoSe<sub>2</sub> on sapphire was transferred onto SiO<sub>2</sub>/Si substrate. Figure 2.7 is schematic description of the wet transfer method by using polymer and sapphire etchant. Previously, HF or KOH, NaOH were used to deep-etch the growth substrate such as sapphire or SiO<sub>2</sub>/Si so as to release the TMDs protected by polymer.<sup>49, 86, 87</sup> In our experiment, PMMA (poly(methyl methacrylate)(PMMA)) was used for protecting layer of MoSe<sub>2</sub>. After the synthesis of MoSe<sub>2</sub> on sapphire, the MoSe<sub>2</sub>/sapphire was covered with PMMA (AR-P 671.04, Allresist) by spin coating (4,000 rpm for 60 sec). The PMMA coated MoSe<sub>2</sub> were peeled off from sapphire during etching of sapphire by the diluted HF solution (10 %). The PMMA/MoSe<sub>2</sub> was washed with fresh DI water several times, finally leaving the PMMA/MoSe<sub>2</sub> floating on the surface of the water and ready for transfer to the SiO<sub>2</sub>/Si substrate. It was confirmed that the MoSe<sub>2</sub> was successfully transferred onto SiO<sub>2</sub> as shown in Figure 2.8a, b. Transferred MoSe<sub>2</sub> to SiO<sub>2</sub>/Si maintains uniform surface and it shows no damage except for wrinkles during transfer process as shown in Figure 2.8b. The different thickness in Figure 2.8c was originated from small molecules such as H<sub>2</sub>O.

MoSe<sub>2</sub> on SiO<sub>2</sub>/Si was fabricated to FET device by e-beam lithography. Figure 2.9 shows a schematic description of fabricating MoSe<sub>2</sub>-based FET device and optical image of the fabricated device with a 1.5 μm of channel length and 2 μm of channel width. Au and Ti were used for electrode and adhesion layer, respectively. Electron transport properties of MoSe<sub>2</sub>-based FET are presented in Figure 2.10. All fabricated FET devices show n-type behavior, which is consistent with previously reported result.<sup>67, 88, 89</sup> The mobility was calculated by using the following equation.

$$\mu(\text{mobility}) = \frac{L}{WC_gV_D} \times \frac{dI_D}{dV_G}$$

L is channel length, W is channel width, C<sub>g</sub> is gate capacitance of SiO<sub>2</sub> 300 nm.<sup>47, 90</sup> The output characteristic of MoSe<sub>2</sub>-based FET device confirms the Ohmic contact with the Au electrodes as shown in Figure 2.10a and 1 V was used for the drain voltage (V<sub>D</sub>) of transport characteristic measurement. The electron transport properties were implemented in a vacuum cryostat connected to a turbo molecular pumping system that maintained below 10<sup>-6</sup> Torr. From the data, the electron mobility was estimated as 0.03 cm<sup>2</sup>/Vs, on/off ratio was found to exceed 10<sup>6</sup> and threshold gate voltage is around 70 volt. After hydrogen plasma reaction, this behavior completely changed. The hydrogenated MoSe<sub>2</sub>-based FET device shows an insulating behavior as shown in Figure 2.10c, d. It is similar to graphene case. Due to the partially hydrogenated MoSe<sub>2</sub>, the electron channel was locally existed. Therefore, electron transfer is difficult to realization.<sup>60, 61</sup>



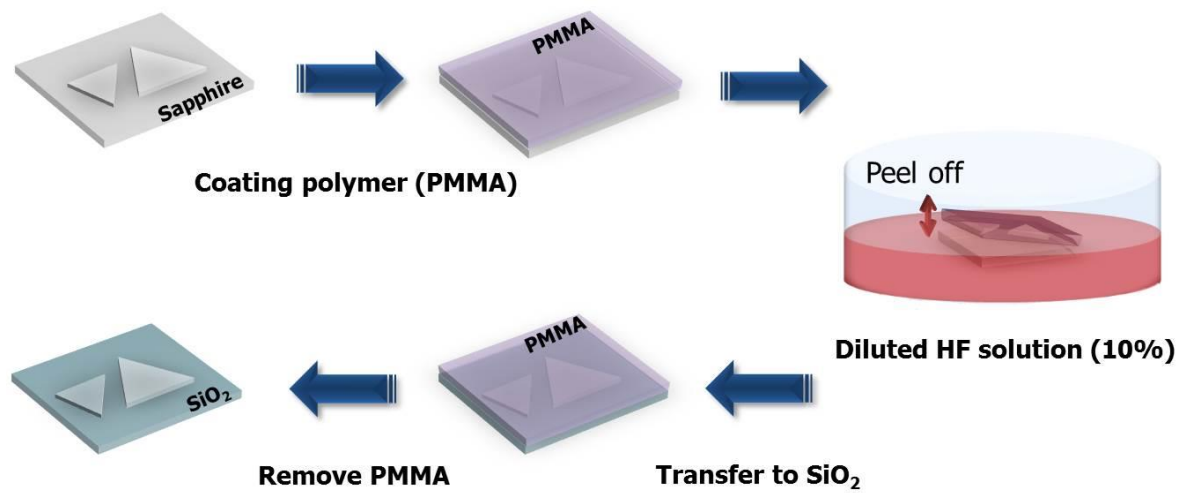


**Figure 2.7** Schematic description of the wet transfer method of MoSe<sub>2</sub> from sapphire to SiO<sub>2</sub>.

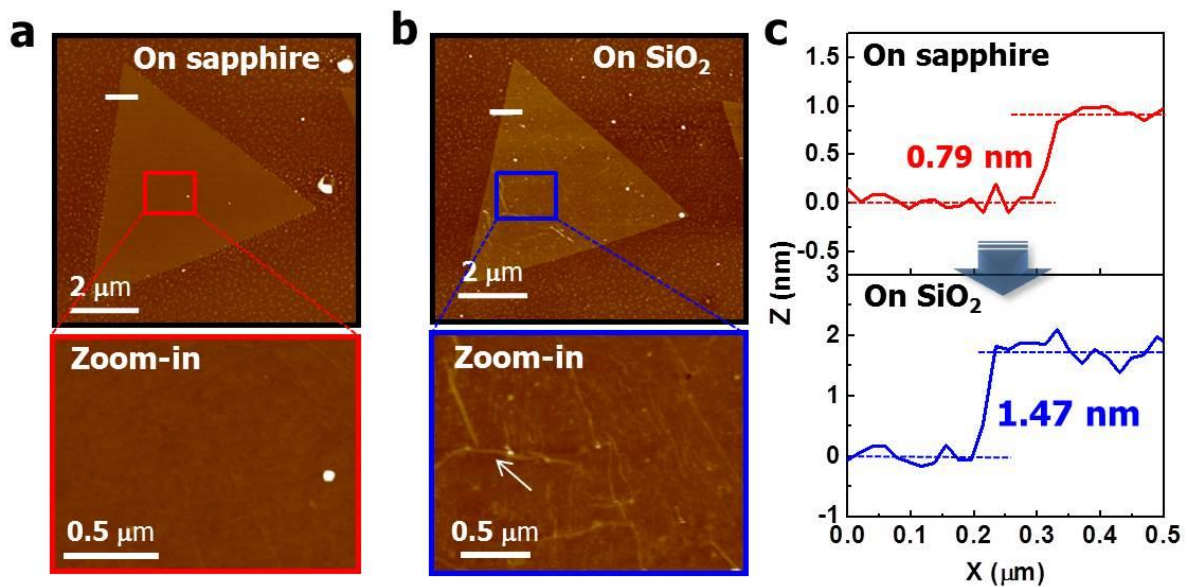


**Figure 2.8** (a) AFM height topography of single-layer MoSe<sub>2</sub> on sapphire and (b) on SiO<sub>2</sub> after transfer. (c) Height profiles of (a) and (b).

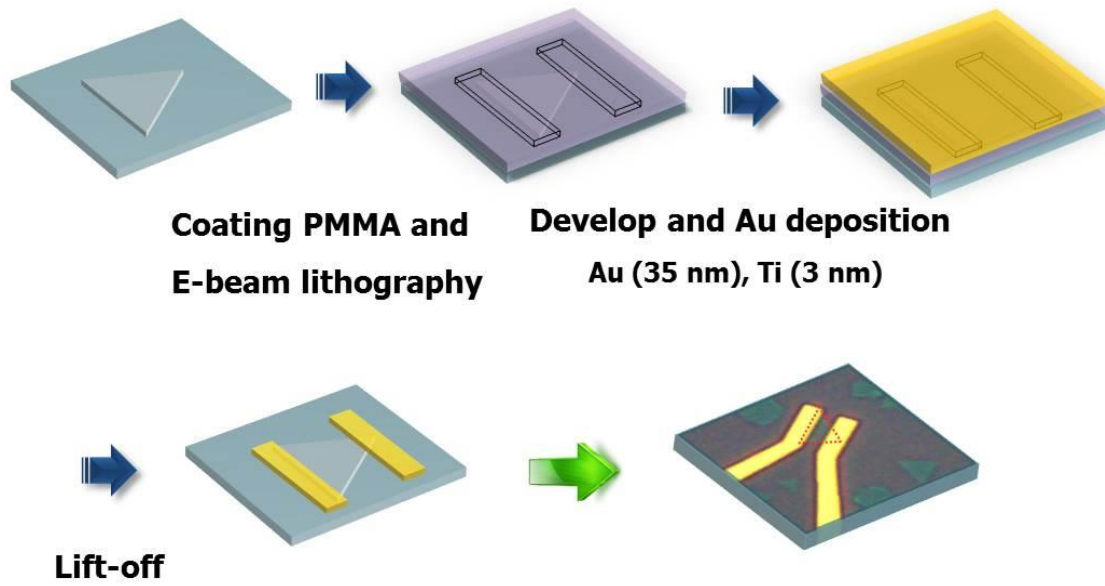


**Figure 2.9** Schematic description of fabricating the back-gate FET device by E-beam lithography.

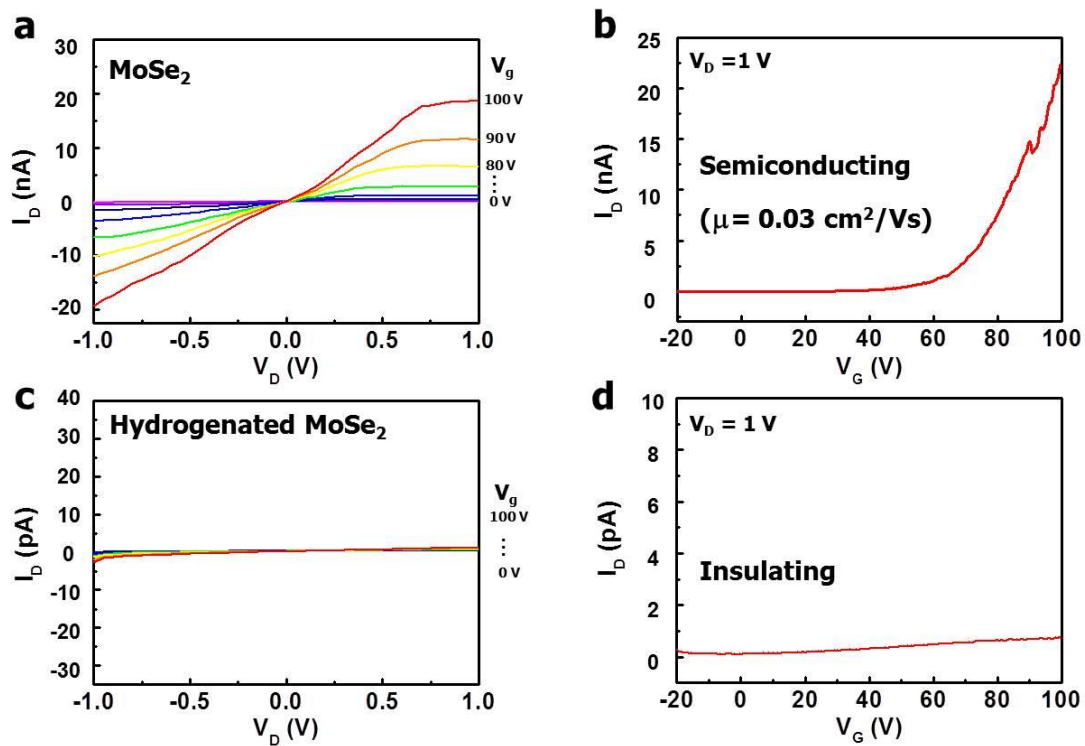


**Figure 2.10** Electron transport characteristics from MoSe<sub>2</sub>-based FET device. (a) I-V curves at different gate voltages and (b) I-V<sub>G</sub> curve in MoSe<sub>2</sub>. (c) I-V curves at different gate voltages and (d) I-V<sub>G</sub> curve in hydrogenated MoSe<sub>2</sub> for more than 168 seconds

### 3.5 Reversible Hydrogenation

In the case of graphene, dehydrogenation is known to be possible by thermal annealing.<sup>60</sup> Due to the thermodynamically unstable state<sup>59, 91</sup> in single sided hydrogenation of ideal graphene, attached hydrogens can be detached by external influences. In our experiment, we tried to restore the optical properties of hydrogenated MoSe<sub>2</sub>. Figure 2.11a and b are PL and Raman of pristine MoSe<sub>2</sub>, respectively, and changes were indicated by PL and Raman after hydrogenation for more than 168 seconds in Figure 2.11c and d. In theoretical study, structure of hydrogenated MoSe<sub>2</sub> is energetically stable.<sup>62, 65</sup> The hydrogenated MoSe<sub>2</sub> showed the same optical characteristics at room temperature for several days in agreement with theoretical result. After thermal annealing at 500 °C in Ar atmosphere for 1 hour, the hydrogenated MoSe<sub>2</sub> was restored. PL and Raman were recovered to practically same state as before hydrogenation (Figure 2.11e, f). However, it was difference to pristine MoSe<sub>2</sub> because vacancies were induced from thermal annealing and plasma damages. This is similar to graphene case.<sup>60</sup>

### 3.6 Hydrogenation of Free-standing MoSe<sub>2</sub>

The hydrogen atom is number one in periodic table, which is the smallest element on earth. And it was known for interstitial atom in material science field. Thus we needed to confirm whether our hydrogenation system on substrate was one-side or both-side. To comparison with the hydrogenation on substrate, we prepared the free-standing MoSe<sub>2</sub>.<sup>92, 93</sup> The membranes have free edges to reduce of strain induced by adsorption of hydrogen.<sup>60</sup> Schematic of hydrogenation on free-standing and on substrate is indicated in Figure 2.12a. Hydrogen atoms attach on both-side on free-standing MoSe<sub>2</sub>. After hydrogenation of free-standing MoSe<sub>2</sub>, the result of change in Raman and PL was similar to react on substrate. However, its saturation time was reduced compare to shift of A<sub>1g</sub> mode in Raman (Figure 2.12b) and fade out of PL at 84 seconds as shown in Figure 2.12d. As a result, it is indicated that the reaction on substrate was one-side reaction and both-side hydrogenation has more highly responsive than one-side reaction.

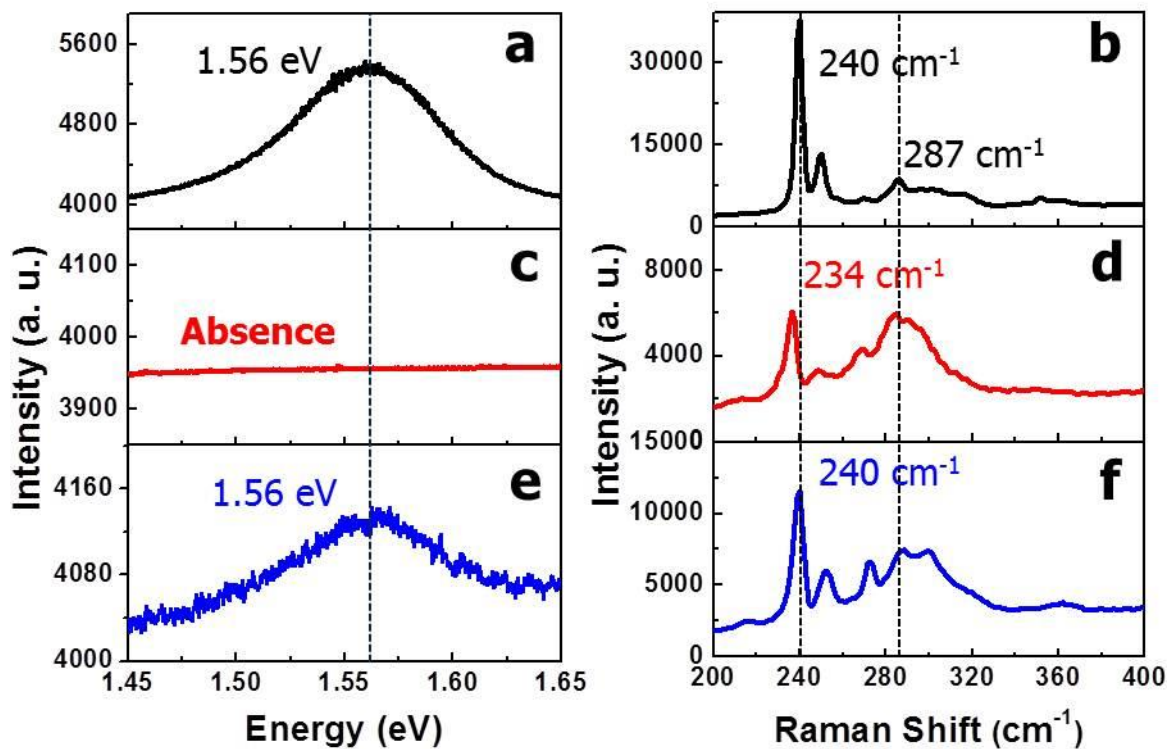


**Figure 2.11** PL and Raman characteristics of dehydrogenation process. Restored PL and Raman spectra are exhibited in (e), (f) from hydrogenated MoSe<sub>2</sub> (c), (d), respectively. The same positions of PL were emitted between pristine MoSe<sub>2</sub> (a) and dehydrogenated MoSe<sub>2</sub> (e). Also peak of A<sub>1g</sub> mode moves to original position of pristine MoSe<sub>2</sub> (f).

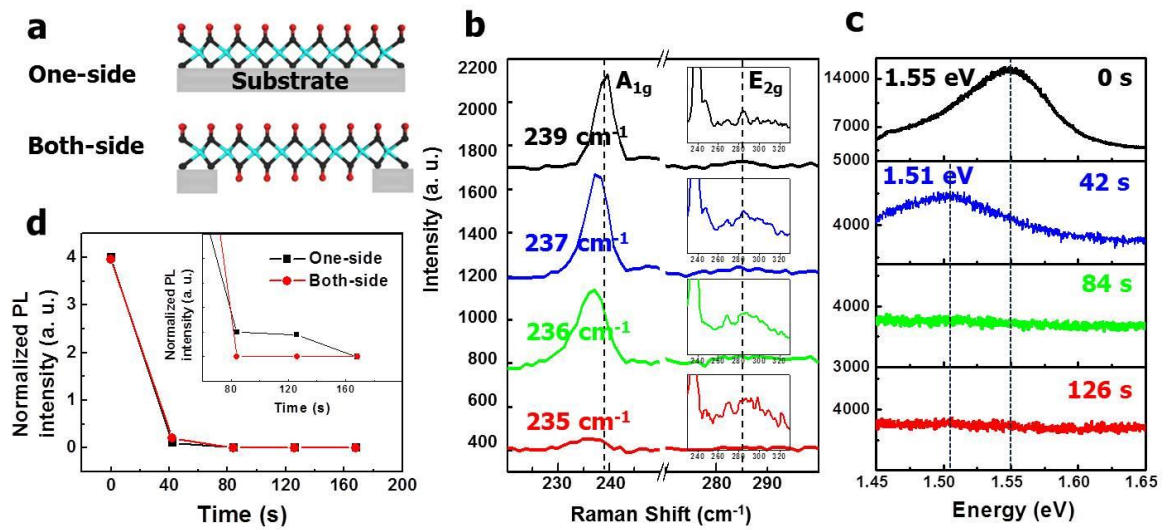


**Figure 2.12** (a) Schematic of one-side and both-side H-MoSe<sub>2</sub>. (b) Raman and (c) PL spectra of both-side H-MoSe<sub>2</sub> with different hydrogenation time. Inset spectra in (b) show magnified E<sub>2g</sub> Raman peak. (d) Normalized PL intensity-time curves of one-side and both-side H-MoSe<sub>2</sub>. Inset in (d) exhibit the magnified curves of from 84 s to 168 s.

#### 4. Summary

In summary, we investigated hydrogenation of single-layer MoSe<sub>2</sub>. Single-layer MoSe<sub>2</sub> was synthesized by CVD method and characterized with Raman, PL, UV-vis-NIR, optical microscopy, SEM, AFM. The radio frequency plasma generator was used for hydrogenation of single-layer MoSe<sub>2</sub> on substrate or free-standing MoSe<sub>2</sub>. After hydrogenation, optical and electrical properties of pristine MoSe<sub>2</sub> were modified. The PL was changed by degree of hydrogenation and initialized hydrogenation from edge area was observed by PL analysis. And MoSe<sub>2</sub>-based FET device show distinct change of electron transport property by hydrogenation from semiconducting to insulating. Also, we could observe the change of Raman spectrum by different hydrogenation time. Through the XPS measurement, we could anticipate that hydrogen is bonded with Se rather than Mo. Similar to graphene case, hydrogenation of MoSe<sub>2</sub> was reversible reaction. By the thermal annealing, Raman and PL properties of hydrogenated MoSe<sub>2</sub> were recovered to pristine MoSe<sub>2</sub>. Finally, we prepared free-standing MoSe<sub>2</sub> to both-side hydrogenation. It shows different hydrogenation efficiency between one-side and both-side by different saturation time and proves the one-side hydrogenation of MoSe<sub>2</sub> on substrate.



## 5. Reference

1. Novoselov, K. S.; Geim, A. K.; Morozov, S. V.; Jiang, D.; Zhang, Y.; Dubonos, S. V.; Grigorieva, I. V.; Firsov, A. A., Electric Field Effect in Atomically Thin Carbon Films. *Science* **2004**, *306*, 666-669.
2. Novoselov, K. S.; Geim, A. K.; Morozov, S. V.; Jiang, D.; Katsnelson, M. I.; Grigorieva, I. V.; Dubonos, S. V.; Firsov, A. A., Two-dimensional gas of massless Dirac fermions in graphene. *Nature* **2005**, *438*, 197-200.
3. Du, X.; Skachko, I.; Duerr, F.; Luican, A.; Andrei, E. Y., Fractional quantum Hall effect and insulating phase of Dirac electrons in graphene. *Nature* **2009**, *462*, 192-195.
4. Han, M. Y.; Özyilmaz, B.; Zhang, Y.; Kim, P., Energy Band-Gap Engineering of Graphene Nanoribbons. *Phys. Rev. Lett.* **2007**, *98*, 206805.
5. Chhowalla, M.; Shin, H. S.; Eda, G.; Li, L.-J.; Loh, K. P.; Zhang, H., The chemistry of two-dimensional layered transition metal dichalcogenide nanosheets. *Nat. Chem.* **2013**, *5*, 263-275.
6. Wilson, J. A.; Yoffe, A. D., The transition metal dichalcogenides discussion and interpretation of the observed optical, electrical and structural properties. *Adv. Phys.* **1969**, *18*, 193-335.
7. Enyashin, A. N.; Yadgarov, L.; Houben, L.; Popov, I.; Weidenbach, M.; Tenne, R.; Bar-Sadan, M.; Seifert, G., New Route for Stabilization of 1T-WS<sub>2</sub> and MoS<sub>2</sub> Phases. *J. Phys. Chem. C* **2011**, *115*, 24586-24591.
8. Brivio, J.; Alexander, D. T. L.; Kis, A., Ripples and Layers in Ultrathin MoS<sub>2</sub> Membranes. *Nano Lett.* **2011**, *11*, 5148-5153.
9. Mak, K. F.; Lee, C.; Hone, J.; Shan, J.; Heinz, T. F., Atomically Thin MoS<sub>2</sub> : A New Direct-Gap Semiconductor. *Phys. Rev. Lett.* **2010**, *105*, 136805.
10. Mattheiss, L. F., Energy Bands for 2H-NbSe<sub>2</sub> and 2H-MoS<sub>2</sub>. *Phys. Rev. Lett.* **1973**, *30*, 784-787.
11. Lebègue, S.; Eriksson, O., Electronic structure of two-dimensional crystals from ab initio theory. *Phys. Rev. B* **2009**, *79*, 115409.
12. Splendiani, A.; Sun, L.; Zhang, Y.; Li, T.; Kim, J.; Chim, C.-Y.; Galli, G.; Wang, F., Emerging Photoluminescence in Monolayer MoS<sub>2</sub>. *Nano Lett.* **2010**, *10*, 1271-1275.
13. Li, T.; Galli, G., Electronic Properties of MoS<sub>2</sub> Nanoparticles. *J. Phys. Chem. C* **2007**, *111*, 16192-16196.
14. Frindt, R. F.; Yoffe, A. D., Physical Properties of Layer Structures: Optical Properties and Photoconductivity of Thin Crystals of Molybdenum Disulphide. *Proc. Roy. Soc. London Ser. A* **1963**, *273*, 69-83.
15. Singh, N.; Jabbour, G.; Schwingenschlögl, U., Optical and photocatalytic properties of two-dimensional MoS<sub>2</sub>. *Eur. Phys. J. B* **2012**, *85*, 1-4.
16. Evans, B. L.; Young, P. A., Optical Absorption and Dispersion in Molybdenum Disulphide. *Proc. Roy. Soc. London Ser. A* **1965**, *284*, 402-422.
17. Coehoorn, R.; Haas, C.; de Groot, R. A., Electronic structure of MoSe<sub>2</sub>, MoS<sub>2</sub>, and WSe<sub>2</sub>. II. The nature of the optical band gaps. *Phys. Rev. B* **1987**, *35*, 6203-6206.
18. Hanke, W.; Sham, L. J., Many-particle effects in the optical spectrum of a semiconductor. *Phys. Rev. B* **1980**, *21*, 4656-4673.



19. Spataru, C. D.; Ismail-Beigi, S.; Benedict, L. X.; Louie, S. G., Excitonic Effects and Optical Spectra of Single-Walled Carbon Nanotubes. *Phys. Rev. Lett.* **2004**, *92*, 077402.
20. Wang, F.; Dukovic, G.; Brus, L. E.; Heinz, T. F., The Optical Resonances in Carbon Nanotubes Arise from Excitons. *Science* **2005**, *308*, 838-841.
21. Arnaud, B.; Lebègue, S.; Rabiller, P.; Alouani, M., Huge Excitonic Effects in Layered Hexagonal Boron Nitride. *Phys. Rev. Lett.* **2006**, *96*, 026402.
22. Kumar, A.; Ahluwalia, P. K., Tunable dielectric response of transition metals dichalcogenides  $\text{MX}_2$  (M=Mo, W; X=S, Se, Te): Effect of quantum confinement. *Phys. B* **2012**, *407*, 4627-4634.
23. Liang, W. Y.; Cundy, S. L., Electron energy loss studies of the transition metal dichalcogenides. *Philos. Mag.* **1969**, *19*, 1031-1043.
24. Mohan, B.; Kumar, A.; Ahluwalia, P. K., A first principle study of interband transitions and electron energy loss in mono and bilayer graphene: Effect of external electric field. *Phys. E* **2012**, *44*, 1670-1674.
25. Coleman, J. N.; Lotya, M.; O'Neill, A.; Bergin, S. D.; King, P. J.; Khan, U.; Young, K.; Gaucher, A.; De, S.; Smith, R. J.; Shvets, I. V.; Arora, S. K.; Stanton, G.; Kim, H.-Y.; Lee, K.; Kim, G. T.; Duesberg, G. S.; Hallam, T.; Boland, J. J.; Wang, J. J.; Donegan, J. F.; Grunlan, J. C.; Moriarty, G.; Shmeliov, A.; Nicholls, R. J.; Perkins, J. M.; Grievson, E. M.; Theuwissen, K.; McComb, D. W.; Nellist, P. D.; Nicolosi, V., Two-Dimensional Nanosheets Produced by Liquid Exfoliation of Layered Materials. *Science* **2011**, *331*, 568-571.
26. Lee, C.; Yan, H.; Brus, L. E.; Heinz, T. F.; Hone, J.; Ryu, S., Anomalous Lattice Vibrations of Single- and Few-Layer  $\text{MoS}_2$ . *ACS Nano* **2010**, *4*, 2695-2700.
27. Kumar, A.; Ahluwalia, P. K., A first principle Comparative study of electronic and optical properties of 1H- $\text{MoS}_2$  and 2H- $\text{MoS}_2$ . *Mater. Chem. Phys.* **2012**, *135*, 755-761.
28. Novoselov, K. S.; Jiang, D.; Schedin, F.; Booth, T. J.; Khotkevich, V. V.; Morozov, S. V.; Geim, A. K., Two-dimensional atomic crystals. *P. Natl. Acad. Sci. Usa.* **2005**, *102*, 10451-10453.
29. Bonaccorso, F.; Lombardo, A.; Hasan, T.; Sun, Z.; Colombo, L.; Ferrari, A. C., Production and processing of graphene and 2D crystals. *Mater. Today* **2012**, *15*, 564-589.
30. Ayari, A.; Cobas, E.; Ogundadegbe, O.; Fuhrer, M. S., Realization and electrical characterization of ultrathin crystals of layered transition-metal dichalcogenides. *J. Appl. Phys.* **2007**, *101*, 014507.
31. Frindt, R. F., Superconductivity in Ultrathin  $\text{NbSe}_2$  Layers. *Phys. Rev. Lett.* **1972**, *28*, 299-301.
32. Staley, N. E.; Wu, J.; Eklund, P.; Liu, Y.; Li, L.; Xu, Z., Electric field effect on superconductivity in atomically thin flakes of  $\text{NbSe}_2$ . *Phys. Rev. B* **2009**, *80*, 184505.
33. Moreno-Moreno, M.; Castellanos-Gomez, A.; Rubio-Bollinger, G.; Gomez-Herrero, J.; Agraït, N., Ultralong Natural Graphene Nanoribbons and Their Electrical Conductivity. *Small* **2009**, *5*, 924-927.
34. RadisavljevicB; RadenovicA; BrivioJ; GiacomettiV; KisA, Single-layer  $\text{MoS}_2$  transistors. *Nat. Nanotechnol.* **2011**, *6*, 147-150.
35. Hernandez, Y.; Nicolosi, V.; Lotya, M.; Blighe, F. M.; Sun, Z.; De, S.; McGovern, I. T.; Holland, B.; Byrne, M.; Gun'Ko, Y. K.; Boland, J. J.; Niraj, P.; Duesberg, G.; Krishnamurthy, S.; Goodhue, R.; Hutchison, J.; Scardaci, V.; Ferrari, A. C.; Coleman, J. N., High-yield production of graphene by liquid-phase exfoliation of graphite. *Nat. Nanotechnol.* **2008**, *3*, 563-568.

36. Zhi, C.; Bando, Y.; Tang, C.; Kuwahara, H.; Golberg, D., Large-Scale Fabrication of Boron Nitride Nanosheets and Their Utilization in Polymeric Composites with Improved Thermal and Mechanical Properties. *Adv. Mater.* **2009**, *21*, 2889-2893.
37. Zeng, Z.; Yin, Z.; Huang, X.; Li, H.; He, Q.; Lu, G.; Boey, F.; Zhang, H., Single-Layer Semiconducting Nanosheets: High-Yield Preparation and Device Fabrication. *Angew. Chem. Int. Ed.* **2011**, *50*, 11093-11097.
38. Zeng, Z.; Sun, T.; Zhu, J.; Huang, X.; Yin, Z.; Lu, G.; Fan, Z.; Yan, Q.; Hng, H. H.; Zhang, H., An Effective Method for the Fabrication of Few-Layer-Thick Inorganic Nanosheets. *Angew. Chem. Int. Ed.* **2012**, *51*, 9052-9056.
39. Joensen, P.; Frindt, R. F.; Morrison, S. R., Single-layer MoS<sub>2</sub>. *Mater. Res. Bull.* **1986**, *21*, 457-461.
40. Benavente, E.; Santa Ana, M. A.; Mendizábal, F.; González, G., Intercalation chemistry of molybdenum disulfide. *Coordin. Chem. Rev.* **2002**, *224*, 87-109.
41. Golub, A. S.; Zubavichus, Y. V.; Slovokhotov, Y. L.; Novikov, Y. N., Single-layer dispersions of transition metal dichalcogenides in the synthesis of intercalation compounds. *Russ. Chem. Rev.* **2003**, *72*, 123-141.
42. Eda, G.; Yamaguchi, H.; Voiry, D.; Fujita, T.; Chen, M.; Chhowalla, M., Photoluminescence from Chemically Exfoliated MoS<sub>2</sub>. *Nano Lett.* **2011**, *11*, 5111-5116.
43. Eda, G.; Fujita, T.; Yamaguchi, H.; Voiry, D.; Chen, M.; Chhowalla, M., Coherent Atomic and Electronic Heterostructures of Single-Layer MoS<sub>2</sub>. *ACS Nano* **2012**, *6*, 7311-7317.
44. Wang, Q. H.; Kalantar-Zadeh, K.; Kis, A.; Coleman, J. N.; Strano, M. S., Electronics and optoelectronics of two-dimensional transition metal dichalcogenides. *Nat. Nanotechnol.* **2012**, *7*, 699-712.
45. Liu, K.-K.; Zhang, W.; Lee, Y.-H.; Lin, Y.-C.; Chang, M.-T.; Su, C.-Y.; Chang, C.-S.; Li, H.; Shi, Y.; Zhang, H.; Lai, C.-S.; Li, L.-J., Growth of Large-Area and Highly Crystalline MoS<sub>2</sub> Thin Layers on Insulating Substrates. *Nano Lett.* **2012**, *12*, 1538-1544.
46. Shi, Y.; Zhou, W.; Lu, A.-Y.; Fang, W.; Lee, Y.-H.; Hsu, A. L.; Kim, S. M.; Kim, K. K.; Yang, H. Y.; Li, L.-J.; Idrobo, J.-C.; Kong, J., van der Waals Epitaxy of MoS<sub>2</sub> Layers Using Graphene As Growth Templates. *Nano Lett.* **2012**, *12*, 2784-2791.
47. Zhan, Y.; Liu, Z.; Najmaei, S.; Ajayan, P. M.; Lou, J., Large-Area Vapor-Phase Growth and Characterization of MoS<sub>2</sub> Atomic Layers on a SiO<sub>2</sub> Substrate. *Small* **2012**, *8*, 966-971.
48. Lee, Y.-H.; Zhang, X.-Q.; Zhang, W.; Chang, M.-T.; Lin, C.-T.; Chang, K.-D.; Yu, Y.-C.; Wang, J. T.-W.; Chang, C.-S.; Li, L.-J.; Lin, T.-W., Synthesis of Large-Area MoS<sub>2</sub> Atomic Layers with Chemical Vapor Deposition. *Adv. Mater.* **2012**, *24*, 2320-2325.
49. Lin, Y.-C.; Zhang, W.; Huang, J.-K.; Liu, K.-K.; Lee, Y.-H.; Liang, C.-T.; Chu, C.-W.; Li, L.-J., Wafer-scale MoS<sub>2</sub> thin layers prepared by MoO<sub>3</sub> sulfurization. *Nanoscale* **2012**, *4*, 6637-6641.
50. Canfield, D.; Parkinson, B. A., Improvement of energy conversion efficiency by specific chemical treatments of molybdenum selenide (n-MoSe<sub>2</sub>) and tungsten selenide (n-WSe<sub>2</sub>) photoanodes. *J. Am. Chem. Soc.* **1981**, *103*, 1279-1281.
51. Chou, S. S.; De, M.; Kim, J.; Byun, S.; Dykstra, C.; Yu, J.; Huang, J.; Dravid, V. P., Ligand Conjugation of Chemically Exfoliated MoS<sub>2</sub>. *J. Am. Chem. Soc.* **2013**, *135*, 4584-4587.

52. Chianelli, R. R.; Siadati, M. H.; De la Rosa, M. P.; Berhault, G.; Wilcoxon, J. P.; Bearden, R.; Abrams, B. L., Catalytic Properties of Single Layers of Transition Metal Sulfide Catalytic Materials. *Catal. Rev.* **2006**, *48*, 1-41.
53. Tuxen, A.; Kibsgaard, J.; Gøbel, H.; Lægsgaard, E.; Topsøe, H.; Lauritsen, J. V.; Besenbacher, F., Size Threshold in the Dibenzothiophene Adsorption on MoS<sub>2</sub> Nanoclusters. *ACS Nano* **2010**, *4*, 4677-4682.
54. Zhou, L.; He, B.; Yang, Y.; He, Y., Facile approach to surface functionalized MoS<sub>2</sub> nanosheets. *RSC Adv.* **2014**, *4*, 32570-32578.
55. Voiry, D.; Goswami, A.; Kappera, R.; SilvaCecilia de Carvalho Castro, e.; Kaplan, D.; Fujita, T.; Chen, M.; Asefa, T.; Chhowalla, M., Covalent functionalization of monolayered transition metal dichalcogenides by phase engineering. *Nat. Chem.* **2015**, *7*, 45-49.
56. Sreeprasad, T. S.; Nguyen, P.; Kim, N.; Berry, V., Controlled, Defect-Guided, Metal-Nanoparticle Incorporation onto MoS<sub>2</sub> via Chemical and Microwave Routes: Electrical, Thermal, and Structural Properties. *Nano Lett.* **2013**, *13*, 4434-4441.
57. Shi, Y.; Huang, J.-K.; Jin, L.; Hsu, Y.-T.; Yu, S. F.; Li, L.-J.; Yang, H. Y., Selective Decoration of Au Nanoparticles on Monolayer MoS<sub>2</sub> Single Crystals. *Sci. Rep.* **2013**, *3*, 1839.
58. Sarkar, D.; Xie, X.; Kang, J.; Zhang, H.; Liu, W.; Navarrete, J.; Moskovits, M.; Banerjee, K., Functionalization of Transition Metal Dichalcogenides with Metallic Nanoparticles: Implications for Doping and Gas-Sensing. *Nano Lett.* **2015**, *15*, 2852-2862.
59. Sofo, J. O.; Chaudhari, A. S.; Barber, G. D., Graphane: A two-dimensional hydrocarbon. *Phys. Rev. B* **2007**, *75*, 153401.
60. Elias, D. C.; Nair, R. R.; Mohiuddin, T. M. G.; Morozov, S. V.; Blake, P.; Halsall, M. P.; Ferrari, A. C.; Boukhalov, D. W.; Katsnelson, M. I.; Geim, A. K.; Novoselov, K. S., Control of Graphene's Properties by Reversible Hydrogenation: Evidence for Graphane. *Science* **2009**, *323*, 610-613.
61. Balog, R.; Jorgensen, B.; Nilsson, L.; Andersen, M.; Rienks, E.; Bianchi, M.; Fanetti, M.; Laegsgaard, E.; Baraldi, A.; Lizzit, S.; Sljivancanin, Z.; Besenbacher, F.; Hammer, B.; Pedersen, T. G.; Hofmann, P.; Hornekaer, L., Bandgap opening in graphene induced by patterned hydrogen adsorption. *Nat. Mater.* **2010**, *9*, 315-319.
62. Tang, Q.; Jiang, D.-e., Stabilization and Band-Gap Tuning of the 1T-MoS<sub>2</sub> Monolayer by Covalent Functionalization. *Chem. Mater.* **2015**, *27*, 3743-3748.
63. He, J.; Wu, K.; Sa, R.; Li, Q.; Wei, Y., Magnetic properties of nonmetal atoms adsorbed MoS<sub>2</sub> monolayers. *Appl. Phys. Lett.* **2010**, *96*, 082504.
64. Ma, Y.; Dai, Y.; Guo, M.; Niu, C.; Lu, J.; Huang, B., Electronic and magnetic properties of perfect, vacancy-doped, and nonmetal adsorbed MoSe<sub>2</sub>, MoTe<sub>2</sub> and WS<sub>2</sub> monolayers. *Phys. Chem. Chem. Phys.* **2011**, *13*, 15546-15553.
65. Zhang, W.; Zhang, Z.; Yang, W., Stability and Electronic Properties of Hydrogenated MoS<sub>2</sub> Monolayer: A First-Principles Study. *J. Nanosci. Nanotechnol.* **2015**, *15*, 8075-8080.
66. Huang, J.-K.; Pu, J.; Hsu, C.-L.; Chiu, M.-H.; Juang, Z.-Y.; Chang, Y.-H.; Chang, W.-H.; Iwasa, Y.; Takenobu, T.; Li, L.-J., Large-Area Synthesis of Highly Crystalline WSe<sub>2</sub> Monolayers and Device Applications. *ACS Nano* **2014**, *8*, 923-930.

67. Wang, X.; Gong, Y.; Shi, G.; Chow, W. L.; Keyshar, K.; Ye, G.; Vajtai, R.; Lou, J.; Liu, Z.; Ringe, E.; Tay, B. K.; Ajayan, P. M., Chemical Vapor Deposition Growth of Crystalline Monolayer MoSe<sub>2</sub>. *ACS Nano* **2014**, *8*, 5125-5131.
68. Horzum, S.; Sahin, H.; Cahangirov, S.; Cudazzo, P.; Rubio, A.; Serin, T.; Peeters, F. M., Phonon softening and direct to indirect band gap crossover in strained single-layer MoSe<sub>2</sub>. *Phys. Rev. B* **2013**, *87*, 125415.
69. Tonndorf, P.; Schmidt, R.; Böttger, P.; Zhang, X.; Börner, J.; Liebig, A.; Albrecht, M.; Kloc, C.; Gordan, O.; Zahn, D. R. T.; Michaelis de Vasconcellos, S.; Bratschitsch, R., Photoluminescence emission and Raman response of monolayer MoS<sub>2</sub>, MoSe<sub>2</sub>, and WSe<sub>2</sub>. *Opt. Express* **2013**, *21*, 4908-4916.
70. Ganatra, R.; Zhang, Q., Few-Layer MoS<sub>2</sub>: A Promising Layered Semiconductor. *ACS Nano* **2014**, *8*, 4074-4099.
71. Xia, J.; Huang, X.; Liu, L.-Z.; Wang, M.; Wang, L.; Huang, B.; Zhu, D.-D.; Li, J.-J.; Gu, C.-Z.; Meng, X.-M., CVD synthesis of large-area, highly crystalline MoSe<sub>2</sub> atomic layers on diverse substrates and application to photodetectors. *Nanoscale* **2014**, *6*, 8949-8955.
72. Zhang, Y.; Chang, T.-R.; Zhou, B.; Cui, Y.-T.; Yan, H.; Liu, Z.; Schmitt, F.; Lee, J.; Moore, R.; Chen, Y.; Lin, H.; Jeng, H.-T.; Mo, S.-K.; Hussain, Z.; Bansil, A.; Shen, Z.-X., Direct observation of the transition from indirect to direct bandgap in atomically thin epitaxial MoSe<sub>2</sub>. *Nat. Nanotechnol.* **2014**, *9*, 111-115.
73. Tongay, S.; Zhou, J.; Ataca, C.; Lo, K.; Matthews, T. S.; Li, J.; Grossman, J. C.; Wu, J., Thermally Driven Crossover from Indirect toward Direct Bandgap in 2D Semiconductors: MoSe<sub>2</sub> versus MoS<sub>2</sub>. *Nano Lett.* **2012**, *12*, 5576-5580.
74. Ross, J. S.; Wu, S.; Yu, H.; Ghimire, N. J.; Jones, A. M.; Aivazian, G.; Yan, J.; Mandrus, D. G.; Xiao, D.; Yao, W.; Xu, X., Electrical control of neutral and charged excitons in a monolayer semiconductor. *Nat. Commun.* **2013**, *4*, 1474.
75. Zhu, Z. Y.; Cheng, Y. C.; Schwingenschlögl, U., Giant spin-orbit-induced spin splitting in two-dimensional transition-metal dichalcogenide semiconductors. *Phys. Rev. B* **2011**, *84*, 153402.
76. Xie, L.; Jiao, L.; Dai, H., Selective Etching of Graphene Edges by Hydrogen Plasma. *J. Am. Chem. Soc.* **2010**, *132*, 14751-14753.
77. Yang, R.; Zhang, L.; Wang, Y.; Shi, Z.; Shi, D.; Gao, H.; Wang, E.; Zhang, G., An Anisotropic Etching Effect in the Graphene Basal Plane. *Adv. Mater.* **2010**, *22*, 4014-4019.
78. Zhang, Y.; Li, Z.; Kim, P.; Zhang, L.; Zhou, C., Anisotropic Hydrogen Etching of Chemical Vapor Deposited Graphene. *ACS Nano* **2012**, *6*, 126-132.
79. Geng, D.; Wu, B.; Guo, Y.; Luo, B.; Xue, Y.; Chen, J.; Yu, G.; Liu, Y., Fractal Etching of Graphene. *J. Am. Chem. Soc.* **2013**, *135*, 6431-6434.
80. Shi, Z.; Yang, R.; Zhang, L.; Wang, Y.; Liu, D.; Shi, D.; Wang, E.; Zhang, G., Patterning Graphene with Zigzag Edges by Self-Aligned Anisotropic Etching. *Adv. Mater.* **2011**, *23*, 3061-3065.
81. Wang, L.; Wu, B.; Jiang, L.; Chen, J.; Li, Y.; Guo, W.; Hu, P.; Liu, Y., Growth and Etching of Monolayer Hexagonal Boron Nitride. *Adv. Mater.* **2015**, *27*, 4858-4864.
82. Sutter, P.; Lahiri, J.; Albrecht, P.; Sutter, E., Chemical Vapor Deposition and Etching of High-Quality Monolayer Hexagonal Boron Nitride Films. *ACS Nano* **2011**, *5*, 7303-7309.

83. Sharma, S.; Kalita, G.; Vishwakarma, R.; Zulkifli, Z.; Tanemura, M., Opening of triangular hole in triangular-shaped chemical vapor deposited hexagonal boron nitride crystal. *Sci. Rep.* **2015**, *5*, 10426.
84. Bougouma, M.; Batan, A.; Guel, B.; Segato, T.; Legma, J. B.; Reniers, F.; Delplancke-Ogletree, M.-P.; Buess-Herman, C.; Doneux, T., Growth and characterization of large, high quality MoSe<sub>2</sub> single crystals. *J. Cryst. Growth* **2013**, *363*, 122-127.
85. Gong, Y.; Liu, Z.; Lupini, A. R.; Shi, G.; Lin, J.; Najmaei, S.; Lin, Z.; Elías, A. L.; Berkdemir, A.; You, G.; Terrones, H.; Terrones, M.; Vajtai, R.; Pantelides, S. T.; Pennycook, S. J.; Lou, J.; Zhou, W.; Ajayan, P. M., Band Gap Engineering and Layer-by-Layer Mapping of Selenium-Doped Molybdenum Disulfide. *Nano Lett.* **2014**, *14*, 442-449.
86. Elías, A. L.; Perea-López, N.; Castro-Beltrán, A.; Berkdemir, A.; Lv, R.; Feng, S.; Long, A. D.; Hayashi, T.; Kim, Y. A.; Endo, M.; Gutiérrez, H. R.; Pradhan, N. R.; Balicas, L.; Mallouk, T. E.; López-Urías, F.; Terrones, H.; Terrones, M., Controlled Synthesis and Transfer of Large-Area WS<sub>2</sub> Sheets: From Single Layer to Few Layers. *ACS Nano* **2013**, *7*, 5235-5242.
87. Zhang, Y.; Zhang, Y.; Ji, Q.; Ju, J.; Yuan, H.; Shi, J.; Gao, T.; Ma, D.; Liu, M.; Chen, Y.; Song, X.; Hwang, H. Y.; Cui, Y.; Liu, Z., Controlled Growth of High-Quality Monolayer WS<sub>2</sub> Layers on Sapphire and Imaging Its Grain Boundary. *ACS Nano* **2013**, *7*, 8963-8971.
88. Larentis, S.; Fallahazad, B.; Tutuc, E., Field-effect transistors and intrinsic mobility in ultra-thin MoSe<sub>2</sub> layers. *Appl. Phys. Lett.* **2012**, *101*, 223104.
89. Lu, X.; Utama, M. I. B.; Lin, J.; Gong, X.; Zhang, J.; Zhao, Y.; Pantelides, S. T.; Wang, J.; Dong, Z.; Liu, Z.; Zhou, W.; Xiong, Q., Large-Area Synthesis of Monolayer and Few-Layer MoSe<sub>2</sub> Films on SiO<sub>2</sub> Substrates. *Nano Lett.* **2014**, *14*, 2419-2425.
90. Liu, H.; Neal, A. T.; Ye, P. D., Channel Length Scaling of MoS<sub>2</sub> MOSFETs. *ACS Nano* **2012**, *6*, 8563-8569.
91. Boukhvalov, D. W.; Katsnelson, M. I.; Lichtenstein, A. I., Hydrogen on graphene: Electronic structure, total energy, structural distortions and magnetism from first-principles calculations. *Phys. Rev. B* **2008**, *77*, 035427.
92. Meyer, J. C.; Geim, A. K.; Katsnelson, M. I.; Novoselov, K. S.; Booth, T. J.; Roth, S., The structure of suspended graphene sheets. *Nature* **2007**, *446*, 60-63.
93. Booth, T. J.; Blake, P.; Nair, R. R.; Jiang, D.; Hill, E. W.; Bangert, U.; Bleloch, A.; Gass, M.; Novoselov, K. S.; Katsnelson, M. I.; Geim, A. K., Macroscopic Graphene Membranes and Their Extraordinary Stiffness. *Nano Lett.* **2008**, *8*, 2442-2446.